Scientific Reports

https://doi.org/10.1038/s41598-025-29725-5

Article in Press

Optimization of biochar production from *Rumex abyssinicus* using response surface methodology and its application in amending degraded soil

Received: 1 October 2025

Accepted: 19 November 2025

Published online: 25 November 2025

Cite this article as: Tibebu S., Worku A., Weldmichael T.G. *et al.* Optimization of biochar production from *Rumex abyssinicus* using response surface methodology and its application in amending degraded soil. *Sci Rep* (2025). https://doi.org/10.1038/s41598-025-29725-5

Solomon Tibebu, Abebe Worku, Tsedekech Gebremeskel Weldmichael & Minbale Aschale

Optimization of Biochar Production from *Rumex abyssinicus* Using Response Surface Methodology and Its Application in Amending Degraded Soil

Solomon Tibebu[a], Abebe Worku[a*], Tsedekech Gebremeskel Weldmichael[a], Minbale Aschale[b]

[a]Department of Environmental Engineering, College of Engineering, Sustainable Energy Center of Excellence, Bioprocess and Biotechnology Center of Excellence, Nanotechnology Center of Excellence, Addis Ababa Science and Technology University, 16417 Addis Ababa, Ethiopia

[b]Bio and Emerging Technology Institute, Addis Ababa, Ethiopia

Corresponding author*: Abebe Worku, abebe.worku@aastu.edu.et, ORCID- 0009-0007-2278-3017

Solomon Tibebu, solomon.tibebu@aastu.edu.et , ORCID-0000-0002-3631-1017 ; Tsedekech Gebremeskel Weldmichael, tsedekech.gebremeskel@aastu.edu.et; Minbale Aschale, minsinas@yahoo.com

Abstract

Soil degradation is a major constraint to agricultural productivity in Ethiopia, particularly in highland regions where erosion, acidity, and nutrient depletion are widespread. Although biochar has shown promise in restoring soil health, its effectiveness depends heavily on feedstock type and production conditions. *Rumex abyssinicus*, a culturally significant and abundant Ethiopian plant, has been studied for activated carbon but not for biochar synthesis or soil rehabilitation using stem biomass. This study addresses that gap by optimizing biochar production from *Rumex. abyssinicus* stems using response surface methodology (RSM), and evaluating its impact on degraded soil. Pyrolysis parameters: temperature, time, heating rate, and particle size, were optimized to maximize yield, achieving 31.98% under ideal conditions. The resulting biochar exhibited high fixed carbon (78.8%), large surface area (455.1 m^2/g), and favorable properties including pHpzc (9.2), WHC (5.56 g/g), and CEC (15 meq/100g). A 100-day pot experiment using soil from Wolayta showed significant improvements in bulk density (−49.24%), porosity (+81.47%), pH (+24.57%), and organic matter (+531.33%). Statistical analysis confirmed treatment effects across key parameters. These findings demonstrate that *Rumex abyssinicus* biochar is a viable, locally sourced amendment for degraded soils. Its use is recommended for sustainable land restoration and climate-resilient agriculture in Ethiopia.

Key words: Biochar; *Rumex abyssinicus*; Pyrolysis optimization; Soil restoration; Response surface methodology; Highland soils

1. Introduction

The degradation of agricultural soils has emerged as a critical global issue, particularly in regions reliant on subsistence farming [1]. In sub-Saharan Africa, extensive soil erosion, nutrient depletion, and organic matter loss are impairing land productivity, undermining food security, and intensifying environmental vulnerability [2]. Ethiopia, in particular, faces acute challenges due to unsustainable land management practices, rapid population growth, and recurrent droughts [3]. Addressing this crisis necessitates the development of low-cost, scalable, and ecologically sound soil restoration approaches.

Among the promising solutions, biochar has gained considerable attention for its potential to enhance soil quality and support sustainable agriculture [4]. Produced via pyrolysis, a thermochemical process that converts biomass into a stable, carbon-rich material under limited oxygen conditions, biochar is known to improve soil structure, nutrient retention, water-holding capacity, and cation exchange capacity (CEC) [5,6]. Additionally, biochar's resistance to microbial degradation contributes to long-term carbon sequestration, offering climate mitigation benefits alongside agronomic gains [7]. However, the performance characteristics of biochar are highly dependent on the feedstock material and pyrolysis parameters, which necessitates systematic optimization for specific applications.

Rumex abyssinicus, a herbaceous plant native to tropical Africa, including Ethiopia, presents an underutilized biomass resource with potential for biochar production [8]. Belonging to the *Polygonaceae* family, *Rumex abyssinicus* is widely distributed across the Ethiopian highlands

[9]. Locally referred to as Gogocha in Amharic and Gogosa in Oromiffa, the plant is well known for its diverse traditional uses, including medicinal, culinary, and dyeing applications [10]. Although *Rumex abyssinicus* has been widely investigated for activated carbon production [11–13], its potential as a biochar feedstock remains largely unexplored, with only one known study addressing this application [8]. This represents a significant research opportunity, especially given the need for regionally appropriate, resource-efficient strategies for soil rehabilitation in degraded landscapes.

To maximize the utility of biochar derived from this species, it is essential to optimize the pyrolysis process to enhance both yield and agronomic functionality [14]. Response Surface Methodology (RSM) offers a robust statistical framework for process optimization, allowing researchers to model the complex interactions between pyrolysis variables such as temperature, residence time, and feedstock particle size [15]. Through RSM, biochar production can be fine-tuned to achieve optimal performance characteristics tailored to specific soil amendment goals.

Despite extensive research on biochar for soil amendment [16–19], no studies to date have investigated the synthesis optimization of biochar derived from *Rumex abyssinicus*, nor its application in soil rehabilitation using stem biomass as feedstock. This represents a critical gap, particularly in the context of Ethiopia's degraded highland soils and the need for locally sourced, cost-effective amendments. Moreover, the use of Response Surface Methodology (RSM) to optimize pyrolysis conditions for this specific biomass has not been previously reported. This study, therefore, aims to (i) optimize biochar production from *Rumex abyssinicus* stems using RSM to maximize yield and agronomic functionality, and (ii) evaluate its effectiveness in improving key soil physicochemical properties. The findings are expected to advance regionally adapted biochar technologies and contribute to sustainable land management strategies in sub-Saharan Africa.

2. Materials and Methods

2.1. Sample Collection and Preparation of Biochar and Degraded Soil

Stems of *Rumex abyssinicus* were harvested from the premises of Addis Ababa Science and Technology University (AASTU), Addis Ababa, Ethiopia. The collected biomass was washed with distilled water to remove surface impurities, oven-dried at 105 °C for 24 h (Model BOV-T50F), and manually chopped. The dried material was milled to uniform particle sizes using a high-speed multifunction mill (Model HC-700) for further processing (Figure 1).

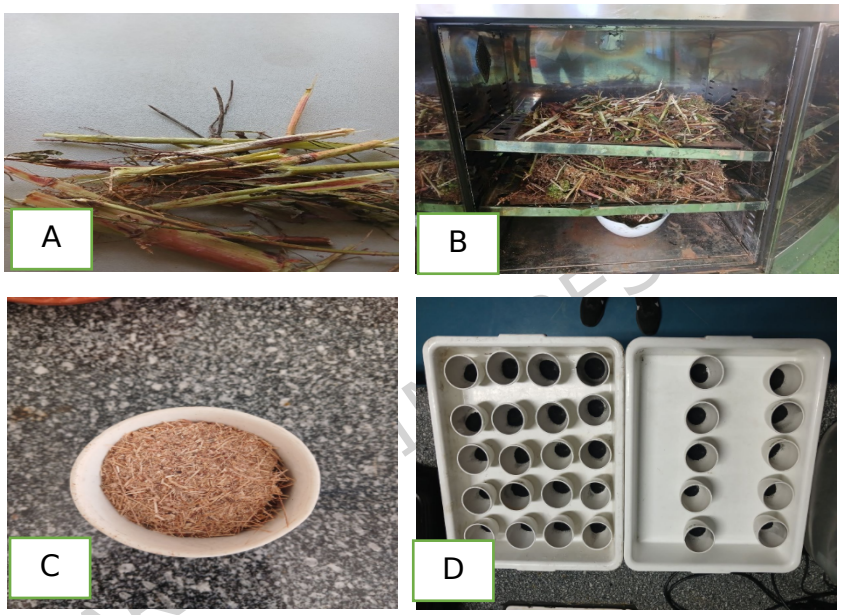

Figure 1. Preparation Stages of Biochar: (A) Steam treatment of *Rumex abyssinicus*, (B) Oven drying, (C) Grinding, and (D) Synthesized biochar experimental runs

Degraded soil samples were collected from Humbo Woreda, located in the Wolaita Zone of the Southern Nations, Nationalities, and Peoples' Region (SNNPR), Ethiopia. The area, situated at 6° N latitude and 37° E longitude, lies within the Great Rift Valley, approximately 330 km southwest of Addis Ababa. It features altitudes ranging from 1,100 to 2,335 m, with an average annual rainfall between 840–1,400 mm and temperatures ranging from 15 to 29 °C. The region's geology is dominated by Precambrian formations, sedimentary layers, and volcanic ash, and its primary soil type is brownish-red clay. Despite its agricultural potential, much of the land is affected by visible degradation and low fertility [20,21]. A 10 m^2

plot of visibly infertile, uncultivated land was selected for soil sampling. The site exhibited sparse vegetation and compacted, poorly aggregated soil, indicators of degradation. The site was intentionally chosen to avoid cultivated land, which may contain synthetic fertilizers or organic amendments, ensuring that the experiment accurately assessed the biochar's amendment potential on naturally degraded soil. As the sampling area was uncultivated and not privately owned or restricted, no formal permission was required for soil collection. Five evenly distributed points across the plot were sampled using a grid method. Surface soil (0–30 cm depth) was collected with a shovel and composited to ensure representativeness [22]. The samples were sealed in airtight plastic bags, transported to the laboratory, and air-dried for one month. Subsequently, the dried soils were ground using a mortar and pestle and passed through a 2 mm sieve prior to characterization.

2.2. Optimization of Biochar Synthesis

Biochar synthesis optimization was conducted using a Central Composite Design (CCD) under Response Surface Methodology (RSM) with 30 experimental runs (6 center and 24 factorial points), designed in Design Expert v13. The number of experiments (M) was calculated using Equation 1.

$$M = 2^{L} + 2L + Bo \quad (1)$$

Where: L denotes the number of factors, and Bo indicates the number of replicates at the central point. For this study, the parameters are defined as follows: M = 30, L = 4, and Bo = 6.

Axial points were positioned face-centered (α=1.0) to ensure rotatability. Experimental runs were randomized to minimize bias. The responses (yield) was modeled using a quadratic polynomial equation (Equation 2). The experimental sequence was randomized to minimize the influence of uncontrolled variables. The resulting data were fitted to a second-order polynomial model to describe the relationship between the response variables and the experimental factors. This quadratic model was used to predict both the biochar yield and

surface area across various parameter combinations. Additionally, the model allowed for evaluating individual effects and interactions among the factors.

$$R = \beta o + \sum_{i=1}^{k} \beta i x i + \sum_{i=1}^{k} \beta i i (x i)^2 + \sum_{i=1}^{k-1} . \sum_{j=i+1}^{k} \beta i j x i x j \quad (2)$$

Where: R represents the predicted response, with β_o denoting the constant coefficient, β_i indicating the coefficients for linear effects, β_{ii} representing the coefficients for quadratic effects, and β_{ij} signifying the coefficients for interaction effects. The variables x_i and x_j correspond to the independent variables, while k represents the total number of independent variables in the equation.

The yield of the synthesized BC was calculated using Equation 3.

$$Y (\%) = \left(\frac{A}{B}\right) * 100 \quad (3)$$

Where: Y represents the yield, B denotes the dry weight of the original sample (mg), and A indicates the dry weight of the synthesized sample (mg).

Carbonization temperature, carbonization time, heating rate, and particle size are considered as factors, with their values fixed according to literature values. The sample pyrolysis was performed in a muffle furnace (Model Naberthem F 330) under an inert atmosphere created by nitrogen gas (N_2 flow rate of 50 mL/min) [23]. The pyrolysis process was conducted at varying carbonization temperatures ranging from 600 °C to 900 °C [24], different carbonization times of 60 min to 120 min [25–27], and heating rates between 10 °C/min and 20 °C/min [28]. Additionally, the particle size of the samples was adjusted between 125 µm to 180 µm [29]. Table 1 presents the factor and their values.

Table 1. Variables Selected for Biochar Synthesis Optimization

Factors	Code	Levels of Coded Variables		
		-1	0	+1
Carbonization Temperature (°C)	CT	600	750	900
Carbonization Time (min)	T	60	90	120

Heating rate (°C/min)	HR	10	15	20
Particle size (µm)	PS	125	150	180

2.3. Effect of Individual Factors

The effect of individual process parameters on biochar yield was systematically examined by varying one factor at a time, while holding the others constant to isolate their respective influences. Carbonization temperature was varied at five levels: 600, 675, 750, 825, and 900 °C. Carbonization time was studied at 60, 75, 90, 105, and 120 minutes. Heating rate was adjusted at 10, 13, 15, 18, and 20 °C/min. Particle size was controlled using standard ASTM E11 test sieves with openings of 106 µm (140 mesh), 125 µm (120 mesh), 150 µm (100 mesh), 180 µm (80 mesh), and 212 µm (70 mesh). These sieve sizes define the maximum particle diameter that can pass through, effectively categorizing the biomass into discrete particle size fractions. For all trials, parameters not under investigation were maintained at their central values: 750 °C for carbonization temperature, 90 minutes for carbonization time, 15 °C/min for heating rate, and 150 µm for particle size.

2.4. Characterization of Synthesized Biochar

Following optimization, bulk quantities of biochar were produced and subjected to comprehensive characterization. The analyses included proximate composition, elemental estimation (C, H, O, N), and surface chemistry assessments. Structural and morphological properties were investigated using X-ray fluorescence (XRF), scanning electron microscopy (SEM), Fourier-transform infrared spectroscopy (FTIR), and X-ray diffraction (XRD). Thermal behavior was evaluated via thermogravimetric analysis (TGA), while surface area was determined using Brunauer-Emmett-Teller (BET) analysis. Additional physicochemical properties, including the point of zero charge (pHpzc), pH, electrical conductivity (EC), bulk density, particle density, specific gravity, water holding capacity (WHC), and cation exchange capacity (CEC), were also measured to assess the suitability of the biochar for soil amendment applications.

2.3.1 Proximate Analysis

Proximate analysis of the biochar was conducted following ASTM standards to determine moisture content, volatile matter, ash content, and fixed carbon. These parameters provide essential information on the thermal stability and composition of the biochar, which influence its performance in environmental applications [13].

2.3.2 Elemental Analysis

Elemental composition (C, H, O, and N) was estimated using empirical correlations derived from proximate analysis data [30]. This approach is useful when direct CHNS/O analysis is unavailable, utilizing fixed carbon, volatile matter, and ash content to calculate elemental percentages, thereby providing a comprehensive compositional profile (Equations 4-7)

$$C\ (wt\%) = 0.635 * FC + 0.460 * VM - 0.095 * AC \quad (4)$$

$$H\ (wt\%) = 0.059 * FC + 0.060 * VM + 0.010 * AC \quad (5)$$

$$O\ (wt\%) = 0.340 * FC + 0.469 * VM - 0.023 * AC \quad (6)$$

$$N\ (wt\%) = 100 - (C + H + O + AC) \quad (7)$$

2.3.3 X-ray Fluorescence (XRF) Analysis

XRF spectroscopy was employed to elucidate the elemental composition and distribution within the biochar. Finely ground samples were pelletized and analyzed using a Thermo Scientific Mobile Test Standard XRF Analyzer at 40 kV and 30 µA. Both major and trace elements were detected across 1–40 keV, with elemental concentrations converted to oxide percentages to represent typical chemical forms present [31].

2.3.4 Scanning Electron Microscopy (SEM)

The surface morphology and microstructural characteristics of the biochar and soil samples were examined using a VEGA3 TESCAN scanning electron microscope operated at an accelerating voltage of 20 kV. Images were captured at a working distance (WD) of approximately 29 mm and a magnification of 500×, with a view field of about 554 µm.

Secondary electron (SE) detection mode was employed to reveal detailed surface topography and porosity features relevant to adsorption capacity and soil structural changes. Scale bars representing 100 µm were included in all micrographs to indicate spatial dimensions. Multiple images at varying magnifications were acquired to comprehensively assess texture, pore distribution, and particle aggregation [32].

2.3.5 Fourier Transform Infrared Spectroscopy (FTIR)

Functional groups present on the biochar surface were identified by FTIR spectroscopy. Samples were mixed with potassium bromide (KBr) in a 2:200 ratio, ground into a homogeneous powder, and pressed into pellets. Spectra were recorded from 4000 to 400 cm^{-1} using a Shimadzu IR Affinity-1s spectrophotometer, revealing chemical bonds responsible for adsorption and reactivity [33].

2.3.6 X-Ray Diffraction (XRD)

XRD analysis was performed to investigate the crystalline and amorphous phases of the biochar. Measurements utilized Cu Kα radiation (λ = 0.15406 nm) over a 2θ range of 10° to 80°, at 40 kV/40 mA with a scanning speed of 4.2°/min. Data analysis enabled phase identification and crystallite size estimation via the Debye-Scherrer equation, providing insights into structural order and stability [34].

2.3.7 Thermogravimetric Analysis (TGA)

To assess the thermal stability and decomposition behavior of biochar intended for soil amendment, thermogravimetric analysis was performed using a Shimadzu DTG-60H analyzer. A 7.444 mg sample was placed in a platinum crucible and heated from 23 °C to 800 °C at a rate of 10 °C/min under a nitrogen atmosphere (flow rate: 50 mL/min). The mass loss profile was recorded to identify key degradation stages and evaluate the structural resilience of the biochar under inert conditions. This thermal characterization was essential for understanding how biochar performed in soil environments, particularly its resistance to breakdown and its potential for long-term carbon retention in degraded soils [35].

2.3.8 Brunauer-Emmett-Teller (BET) Surface Area Analysis

The surface area of the biochar was measured using the BET method with a Horiba SA-9600 analyzer. Approximately 0.4 g of sample was degassed at 100 °C for 2 hours before nitrogen adsorption/desorption analysis at 700 mm atmospheric pressure, providing key porosity and surface property data [36].

2.3.9 Point of Zero Charge (pH_{PZC})

The pH at the point of zero charge (pH_{PZC}) was determined via the salt addition method. Biochar samples (0.5 g) were equilibrated with 0.01 M NaCl solutions adjusted to initial pH values from 2 to 12. After 36 hours of shaking at 25 ± 1 °C, final pH values were recorded. The pHpzc corresponds to the point where initial and final pH values intersect, indicating the surface charge neutrality of the biochar [37].

2.3.10 pH and Electrical Conductivity (EC)

pH and EC measurements were conducted in a 1:5 biochar-to-distilled water suspension. After shaking for 30 minutes and equilibrating for 1 hour, measurements were taken with calibrated portable meters. Triplicate analyses ensured reliability, with the averaged data reported as [38].

2.3.11 Bulk Density, Particle Density, and Specific Gravity

Bulk density was calculated by measuring dry mass and volume using the core method. Particle density was determined through ethanol displacement, measuring volume changes upon immersion. Specific gravity was computed as the ratio of particle density to water density at 4 °C, providing insight into packing and porosity characteristics [39].

2.3.12 Water Holding Capacity (WHC)

WHC was assessed gravimetrically by saturating 5 g of oven-dried biochar with deionized water, allowing drainage for 24 hours at room temperature, then drying at 105 °C. The difference between wet and dry weights quantified the biochar's water retention capacity, critical for soil amendment applications [40].

2.3.13 Cation Exchange Capacity (CEC)

CEC was measured using an equilibrium pH method, involving treatment of 1 g biochar with 25 mL of 1 M acetic acid under stirring for 1 hour. The pH difference between the solution and acetic acid blank was used with a conversion factor to calculate CEC, indicating nutrient retention potential [41].

2.5. Characterization of Degraded Soil

Physicochemical characterization of the degraded soil was carried out to evaluate its fertility status, structural integrity, and suitability for biochar amendment. Key parameters such as bulk density, moisture content, cation exchange capacity, and nutrient availability were analyzed using standardized laboratory techniques. These measurements are essential for establishing baseline conditions and assessing the effects of biochar application. Table 2 summarizes the instruments and methods used to characterize soil samples using basic physicochemical parameters.

Table 2. Soil sample parameters with their respective methods for characterization

No.	Parameter	Instrument/Equipment	Standard Method	Reference
1	Bulk Density	Core Sampler, Balance	Core Method	[42]
2	Particle Density	Graduated cylinder, Balance	Liquid Displacement Method	[42]
3	Specific Gravity	Calculated from Particle Density and Water Density	Ratio of Particle Density to Water Density	[42]
4	Porosity	Graduated Cylinder, Balance, Water (or Mercury)	Water displacement Method	[42]
5	Moisture Content	Oven, Balance	Gravimetric Method	[43]
6	Water Holding Capacity	Saturation Setup, Balance, Oven	Gravimetric Method after Saturation	[44]

7	pH	pH Meter	1:2.5 Soil: Water Suspension	[45]
8	Electrical Conductivity (EC)	EC Meter	1:2.5 Soil: Water Suspension	[46]
9	Cation Exchange Capacity (CEC)	pH Meter, Magnetic Stirrer, Glass Beaker	Equilibrium pH Shift Method using 1 M Acetic Acid	[47]
10	Organic Matter (OM)	Muffle Furnace, Balance	Loss on Ignition	[48]
11	Total Kjeldahl nitrogen (TKN)	Kjeldahl Apparatus	Modified Kjeldahl Digestion	[49]
12	Available Phosphorus (P)	Spectrophotometer (Molybdenum Blue Method)	Olsen P Method ($NaHCO_3$ Extraction)	[50]
13	Available Potassium (K)	Flame Photometer	1 M Ammonium Acetate Extraction (pH 7.0)	[51]
14	Exchangeable Sodium (Na)	Flame Photometer	1 M Ammonium Acetate Extraction (pH 7.0)	[52]
15	Exchangeable Calcium (Ca)	Flame Photometer	1 M Ammonium Acetate Extraction (pH 7.0)	[52]
16	Exchangeable Acidity ($H^+ + Al^{3+}$)	Titration	1 M KCl Extraction	[53]
17	Soil Texture	Sieve, Hydrometer, Pipette	Hydrometer	[54]

2.6. Soil Amendment Experiment

The amendment potential of biochar (BC) was assessed through a 100-day outdoor pot incubation experiment under natural sunlight conditions [55]. This setup aimed to simulate

field-relevant environmental conditions while evaluating the effects of BC on key soil physicochemical properties. Air-dried, homogenized degraded soil (1 kg per treatment) was amended with different BC application rates: 0% (control), 10%, 15%, and 20% by weight [56,57]. The biochar used for amendment was produced under the optimized pyrolysis conditions identified in Section 3.4. The amended soils were thoroughly mixed and transferred into 9.43-liter polyethylene pots (20 cm diameter × 30 cm height). To maintain soil moisture consistent with natural field conditions, deionized water was added twice weekly at a rate of 30 mL per pot, equating to approximately 50% of estimated field capacity. The use of deionized water ensured no external ions were introduced, preserving the native soil chemistry.

At the end of the incubation period, soil samples from each treatment were analyzed in triplicate for physicochemical properties, including bulk density, particle density, specific gravity, porosity, moisture content, water holding capacity, pH, electrical conductivity (EC), cation exchange capacity (CEC), and organic matter (OM). These replicated analyses ensured statistical reliability and supported robust comparison of treatment effects.

3. Results and Discussion

3.1. Synthesis Optimization of Biochar

The optimization of *Rumex abyssinicus*-derived biochar synthesis was performed using RSM, considering four independent process variables: carbonization temperature, residence time, heating rate, and particle size. The experimental matrix, consisting of 30 runs (Table 3), was designed to systematically evaluate their influence on biochar yield. The experimental results demonstrated a narrow variation in yield, ranging from 28.21% to 31.98%, with the highest yield obtained at Run 9, corresponding to a carbonization temperature of 600 °C, a residence time of 120 minutes, a heating rate of 20 °C/min, and a particle size of 180 µm.

The observed increase in yield at moderate carbonization temperature (600 °C) with prolonged residence time aligns with the thermochemical behavior of lignocellulosic

biomass, where extended exposure facilitates complete devolatilization and solid char formation without excessive thermal degradation [58]. Additionally, the selected heating rate (20 °C/min) likely provided a balance between thermal diffusion and reaction kinetics, preventing structural collapse or excessive tar formation, both of which can reduce solid yield [59]. The finer particle size (180 µm) may have enhanced thermal uniformity during pyrolysis, contributing to improved mass and heat transfer efficiency [60].

A comparison between the actual and predicted values showed a high level of agreement, with minimal deviation across all runs, indicating the robustness of the developed RSM model. The optimized condition (Run 9) was selected for subsequent characterization and application studies, as it provided the maximum biochar yield under thermally practical and scalable conditions. These findings highlight the importance of tuning operational parameters collectively, as the interaction effects between temperature, time, heating rate, and particle size can significantly influence the biochar yield even in the absence of chemical activation or catalysts.

Table 3. Optimization of Biochar Synthesis

Run	Carbonization Temperature (°C)	Carbonization Time (min)	Heating Rate (°C/min)	Particle Size (µm)	Yield (%)	
					Actual Value	Predicted Value
1	750	90	15	125	30.225	30.40
2	600	60	10	180	31.69	31.71
3	600	60	10	125	31.66	31.39
4	750	90	20	150	31.53	31.33
5	750	90	10	150	31.54	31.73
6	750	90	15	180	31.43	31.25
7	750	90	15	150	30.19	30.22
8	600	60	20	125	30.13	30.17
9	**600**	**120**	**20**	**180**	**31.98**	**32.00**
10	900	60	20	180	30.17	30.03
11	750	90	15	150	30.28	30.22
12	600	120	20	125	31.31	31.21
13	900	120	20	125	28.61	28.63
14	900	120	20	180	29.79	30.02
15	750	60	15	150	28.56	28.69

16	900	60	10	180	31.74	31.82
17	750	90	15	150	30.06	30.22
18	600	60	20	180	30.7	30.77
19	900	90	15	150	29.82	29.68
20	750	90	15	150	30.37	30.22
21	900	120	10	180	29.58	29.56
22	600	90	15	150	30.81	30.94
23	900	120	10	125	28.543	28.45
24	750	120	15	150	28.21	28.07
25	900	60	10	125	30.89	30.90
26	900	60	20	125	28.78	28.84
27	600	120	10	125	30.03	30.19
28	600	120	10	180	30.78	30.70
29	750	90	15	150	30.12	30.22
30	750	90	15	150	30.26	30.22

This study was compared with previous investigations on biochar production from different biomass sources under varying carbonization conditions, as summarized in Table 4.

Table 4. Comparison of biochar yields from various biomass sources under different carbonization conditions

Biomass Source	**Carbonization Temperature (°C)**	**Carbonization Time (min)**	**Heating Rate (°C/min)**	**Particle Size (µm)**	**Yield (%)**	**Reference**
Rice husk	400	30	-	-	38.5	[61]
Eucalyptus Saw Dust	300	-	5	425	41.9	[62]
Eucalyptus Chips	400	-	5	300	32.2	[62]
Sewage Sludge	500	-	5	250	65.3	[62]
Spent coffee grounds	350	20	5	710	48.35	[63]
Prosepis Juliflora	400	-	10	-	46.53	[64]
Prosepis Juliflora	500	-	10	-	40.24	[64]
Prosepis Juliflora	600	-	10	-	36.38	[64]
Rice Straw Segment	600	-	5	-	32.0	[65]
Water buffalo manure	350	-	10	-	47.0	[66]
Rumex abyssinicus	600	120	20	180	31.98	This study

Although the yield from *Rumex abyssinicus* biochar (31.98%) appears lower than some reported values, it reflects a deliberate optimization of carbonization parameters aimed at

enhancing structural stability and surface functionality. Elevated temperature (600 °C) and extended residence time (120 min) promote devolatilization, reducing bulk yield but improving fixed carbon content and porosity, attributes essential for environmental applications. This biochar was specifically engineered and applied as a soil amendment for degraded soils, where its physicochemical properties contribute to improved retention, nutrient availability, and long-term carbon sequestration. The trade-off between yield and functionality is therefore justified by its targeted role in soil rehabilitation.

3.2. ANOVA and Development of the Regression Model Equation

The statistical robustness of the regression model was assessed using analysis of variance (ANOVA), as presented in Table 5. This analysis evaluates the significance of individual model terms and their interactions, guiding the refinement of the predictive model for biochar yield.

Table 5. Analysis of variance (ANOVA) for the quadratic regression model of biochar yield

Source	Sum of squares	df	Mean of square	F-value	P-value	
Model	31.41	14	2.24	69.66	< 0.0001	significant
A-Carbonization Temperature	6.89	1	6.89	214.02	< 0.0001	
B-Carbonization Time	1.67	1	1.67	51.76	< 0.0001	
C-Heating Rate	0.6575	1	0.6575	20.41	0.0004	
D-Particle Size	3.28	1	3.28	101.79	< 0.0001	
AB	1.55	1	1.55	48.07	< 0.0001	
AC	0.7069	1	0.7069	21.95	0.0003	
AD	0.3639	1	0.3639	11.30	0.0043	
BC	5.01	1	5.01	155.68	< 0.0001	
BD	0.0373	1	0.0373	1.16	0.2986	
CD	0.0768	1	0.0768	2.38	0.1434	
A^2	0.0234	1	0.0234	0.7268	0.4073	
B^2	8.72	1	8.72	270.85	< 0.0001	
C^2	4.48	1	4.48	139.11	< 0.0001	
D^2	0.8371	1	0.8371	25.99	0.0001	
Residual	0.4831	15	0.0322			
Lack of Fit	0.4192	10	0.0419	3.28	0.1011	not significant

Pure Error	0.0639	5	0.0128
Cor Total	31.89	29	

The statistical analysis of the quadratic regression model reveals a Model F-value of 69.66, indicating that the model is highly significant, with only a 0.01% probability that such a large F-value could arise due to random noise. Among the model terms, factors A (carbonization temperature), B (carbonization time), C (heating rate), D (particle size), and their interactions AB, AC, AD, BC, along with the quadratic terms B^2, C^2, and D^2, were statistically significant with p-values less than 0.05, confirming their substantial influence on biochar yield. In contrast, terms with p-values exceeding 0.10 are considered insignificant and may be candidates for removal to improve model simplicity and predictive accuracy, provided they are not required to preserve model hierarchy. The Lack of Fit F-value of 3.28 suggests that lack of fit is not significant relative to pure error, with a 10.11% probability that such a value could be due to noise, indicating that the model fits the experimental data well. Furthermore, the Predicted R^2 value of 0.9165 shows strong agreement with the Adjusted R^2 of 0.9707, with a difference well below the 0.2 threshold, validating the model's predictive strength. The Adequate Precision ratio of 30.925 exceeds the minimum desirable value of 4, demonstrating a high signal-to-noise ratio and confirming that the model is suitable for navigating the design space. The final regression model, expressed in terms of coded variables, is presented in Equation (8) and describes the relationship between the process parameters and the predicted biochar yield.

$$Y\,(\%) = 30.25 - 0.6189A - 0.3043B - 0.1911C + 0.4268D - 0.3111AB - 0.2102AC + 0.1507AD + 0.5598BC + 0.0483BD + 0.0693CD + 0.0951A^2 - 1.83B^2 + 1.32C^2 + 0.5735D^2 \quad (8)$$

The reliability and robustness of the developed quadratic regression model for predicting biochar yield were assessed using diagnostic plots. Figure 2A (Predicted vs. Actual values) illustrates a strong linear relationship, indicating that the model accurately predicts the experimental data, with minimal deviation from the ideal 45-degree line. This alignment signifies high model accuracy and low prediction error. Figure 2B (Residuals vs. Run order)

evaluates the randomness of residual distribution across the experimental runs. The absence of discernible patterns confirms that the residuals are independently and randomly distributed, which validates the assumption of constant variance and model stability throughout the design space. Figure 2C (Residuals vs. Predicted values) further tests the homoscedasticity of the model; the uniform scatter around zero without funneling or curvature suggests that the variance of residuals remains constant over the prediction range. Collectively, these diagnostic plots validate the adequacy of the model and affirm its suitability for navigating the experimental design space.

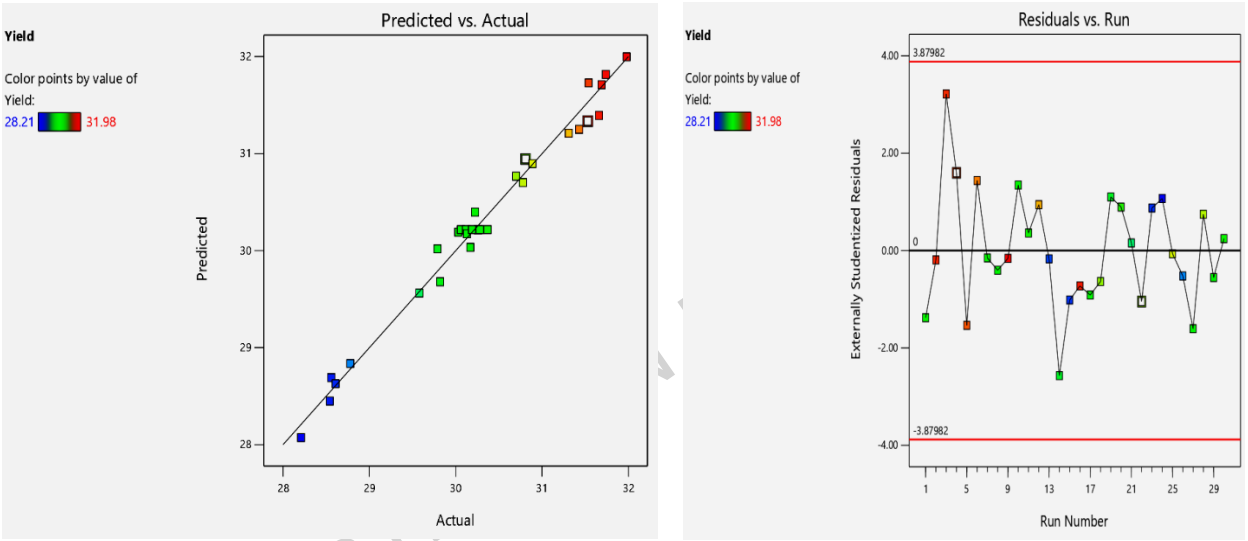

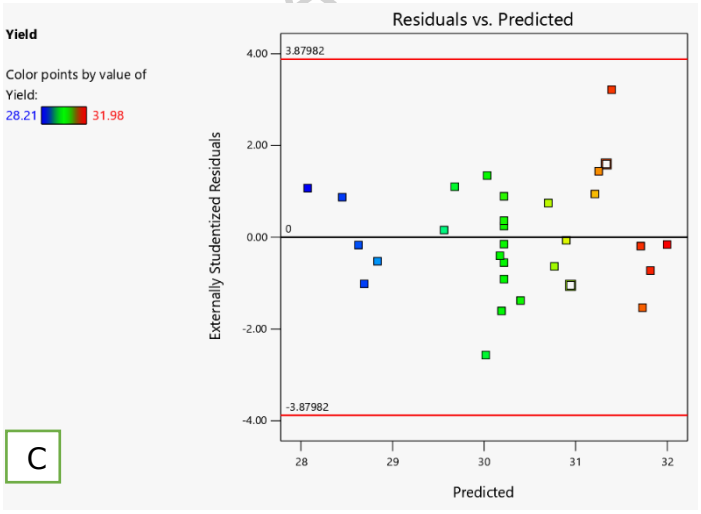

Figure 2.Diagnostic plots for regression model adequacy in biochar yield prediction: (A) Predicted vs. Actual yield showing excellent agreement, (B) Residuals vs. Run order confirming random distribution, and (C) Residuals vs. Predicted values indicating constant variance and no bias

3.3. The Effect of Factors' Interaction on Biochar Yield

The interaction between carbonization temperature and carbonization time had a pronounced influence on biochar yield, as supported by the significant interaction term AB ($p < 0.0001$). Yield increased when both temperature and time were raised to an optimal range, after which further increases, particularly in temperature, led to a decline. This behavior is associated with the thermal decomposition characteristics of lignocellulosic biomass, where moderate temperatures (~750 °C) allow adequate volatile release and biochar formation, while excessive temperatures near 900 °C promote secondary cracking and degradation of the fixed carbon, reducing solid yield [67]. Additionally, longer carbonization times enhance devolatilization, but at very high temperatures, prolonged exposure exacerbates carbon loss through combustion or secondary reactions [68]. These synergistic effects are visually presented in Figure 3, showing a dome-shaped surface where the peak biochar yield lies within the mid-range of both factors.

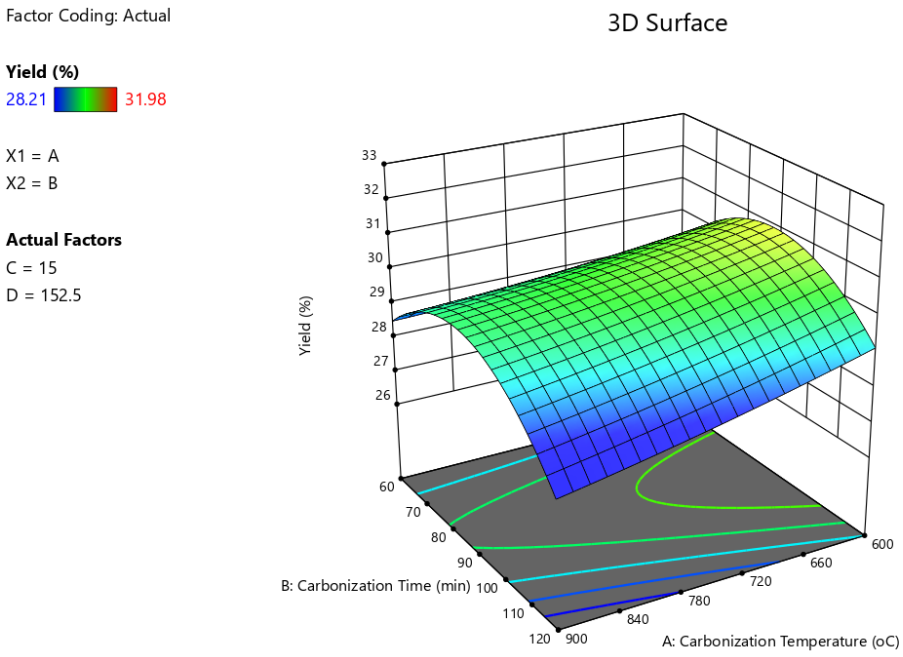

A

401

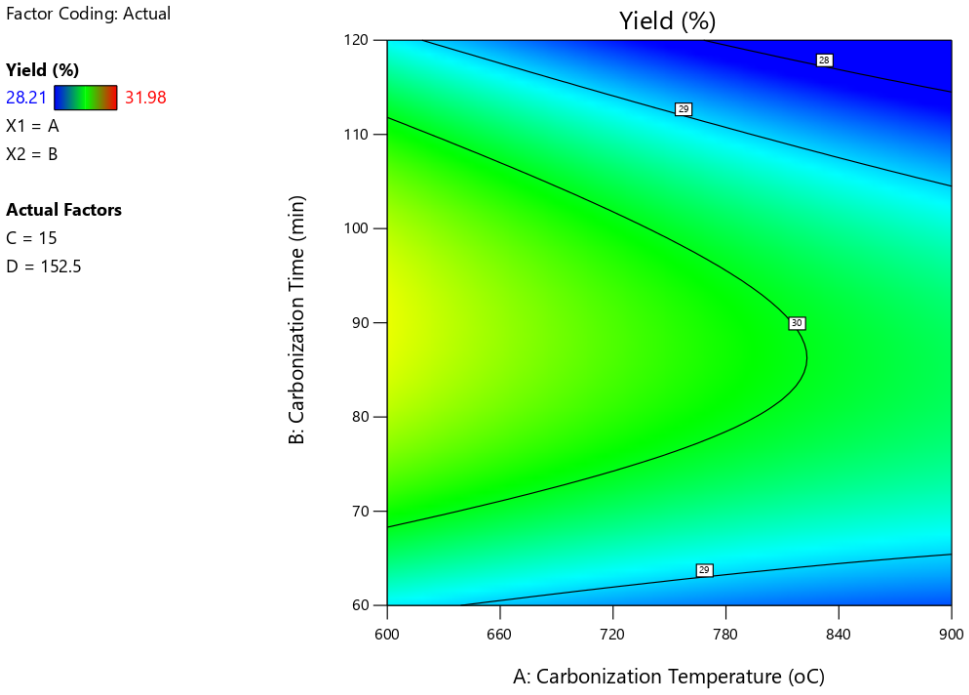

B

402

403 Figure 3. Interaction between Carbonization Temperature and Carbonization Time on

404 biochar yield: (A) 3D surface plot and (B) contour plot.

A statistically significant interaction was also observed between carbonization temperature and heating rate (term AC, $p = 0.0003$). Yield improved with increasing temperature, particularly at a moderate heating rate of around 15 °C/min. However, at higher heating rates, the yield began to drop despite elevated temperatures. This is likely due to uneven thermal diffusion in the biomass structure during rapid heating, which can lead to incomplete carbonization, formation of tar, and potential collapse of the porous matrix [69]. At the optimal heating rate, thermal transfer is sufficiently balanced with reaction kinetics, supporting efficient char formation without overheating the sample. The influence of this interaction is illustrated in Figure 4, which depicts a curved surface response where excessive heating rate beyond a threshold negates the benefits of high carbonization temperature.

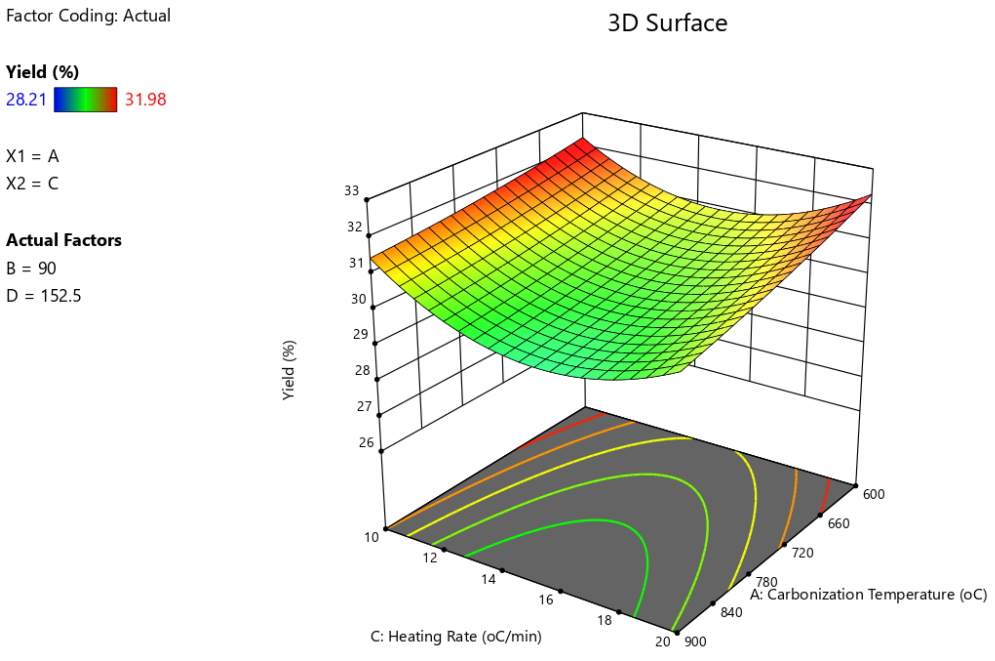

A

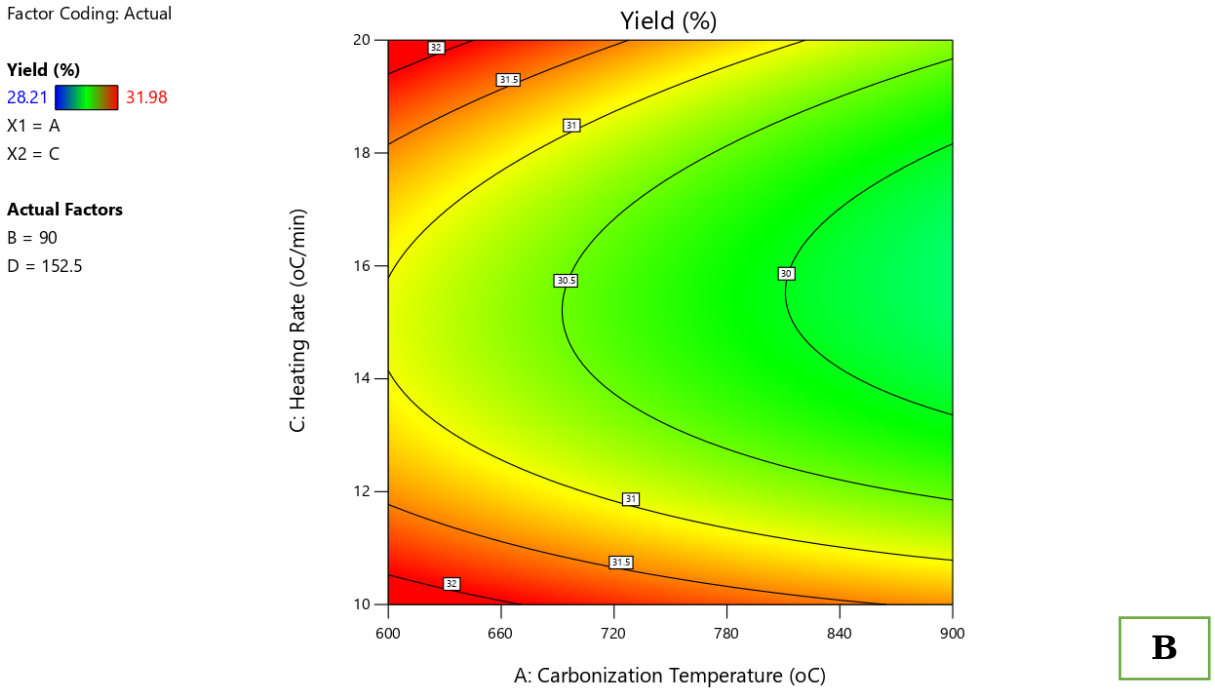

Figure 4. Interaction between Carbonization Temperature and Heating Rate on biochar yield: (A) 3D surface plot and (B) contour plot

The effect of carbonization temperature and particle size interaction (term AD, $p = 0.0043$) highlights the importance of particle geometry in thermal processing. As shown in Figure 5, finer particles (around 125 µm) resulted in higher biochar yields, especially when coupled with increasing temperatures. The increased surface area and reduced diffusion resistance of small particles enhance heat penetration and volatile escape, which promotes a more controlled pyrolysis process and limits tar deposition or incomplete charring [70]. In contrast, coarser particles (180 µm) experience slower heat transfer, leading to heterogeneity in thermal decomposition and a drop in yield at higher temperatures due to insufficient inner-core conversion [71]. This interaction suggests that optimizing particle size is crucial for ensuring uniform carbonization, particularly when operating at elevated temperatures.

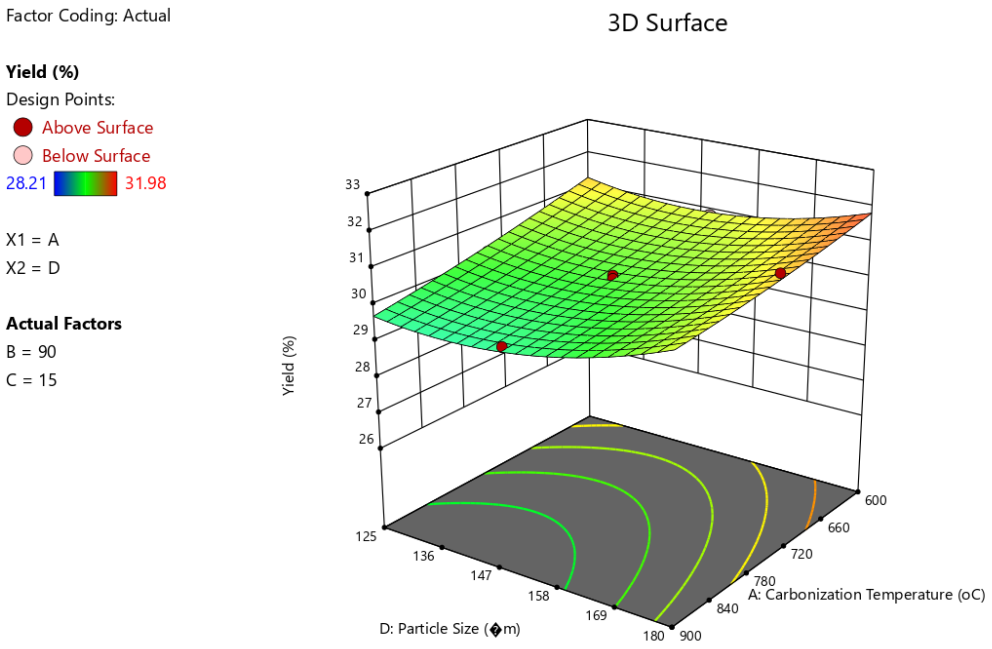

A

429

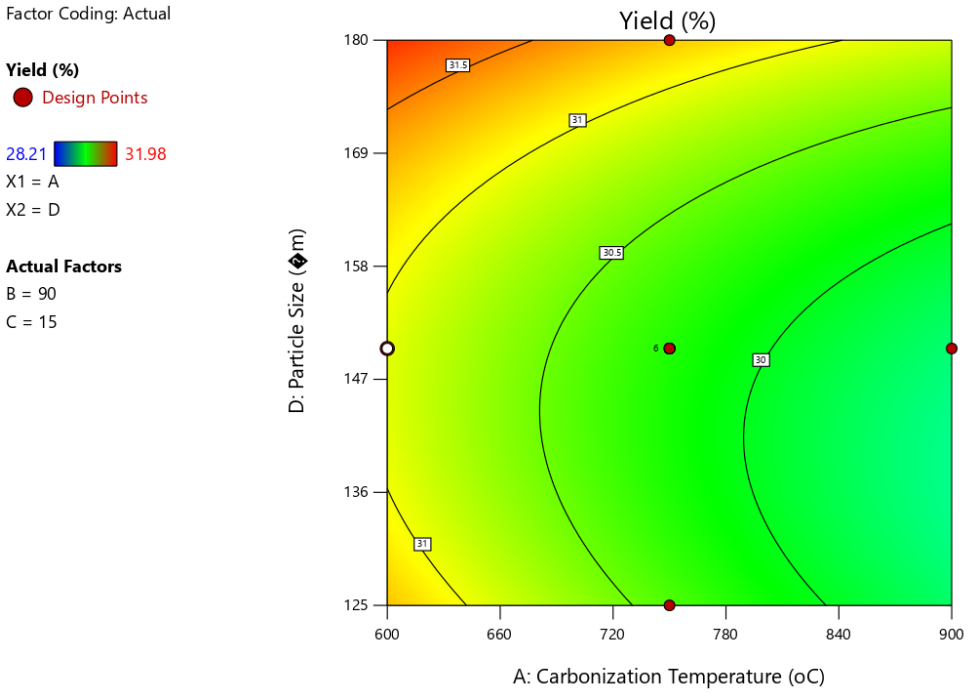

B

430

431 Figure 5. Interaction between Carbonization Temperature and Particle Size on biochar yield:

432 (A) 3D surface plot and (B) contour plot

The interaction between carbonization time and heating rate was highly significant (term BC, $p < 0.0001$), indicating a strong dependency between these variables. As reflected in Figure 6, increasing carbonization time generally enhanced yield at low to moderate heating rates (10–15 °C/min). Longer durations provide more opportunity for primary pyrolysis reactions to complete, especially under slower heating conditions that prevent thermal shock or structural degradation [72]. However, at high heating rates (20 °C/min), the effect of time becomes less influential, as the rapid temperature rise leads to flash devolatilization and limited thermal uniformity, negating the benefits of prolonged residence time [73]. This observation suggests that the heating rate must be carefully calibrated with time to maintain thermal control and avoid premature loss of carbon content.

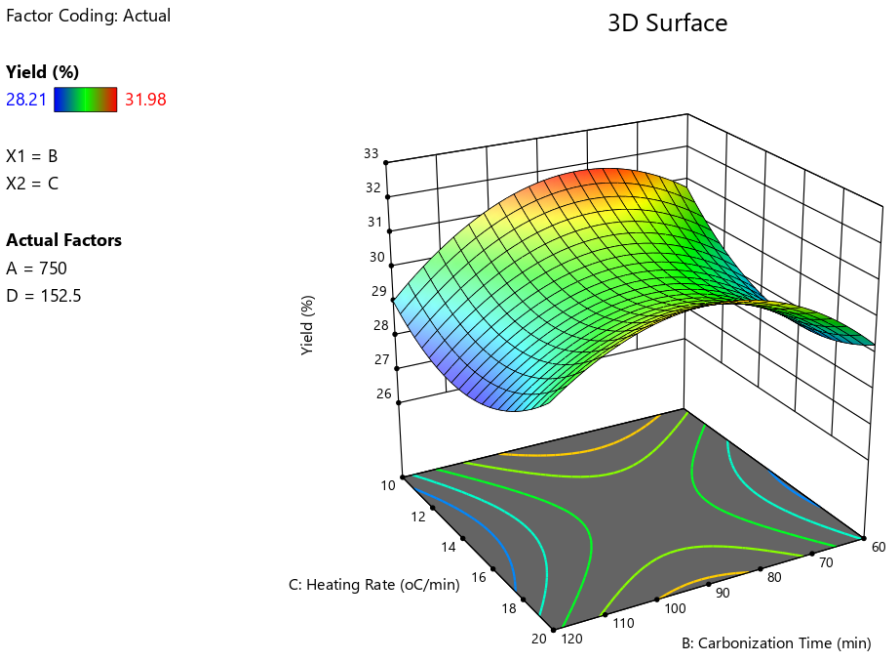

A

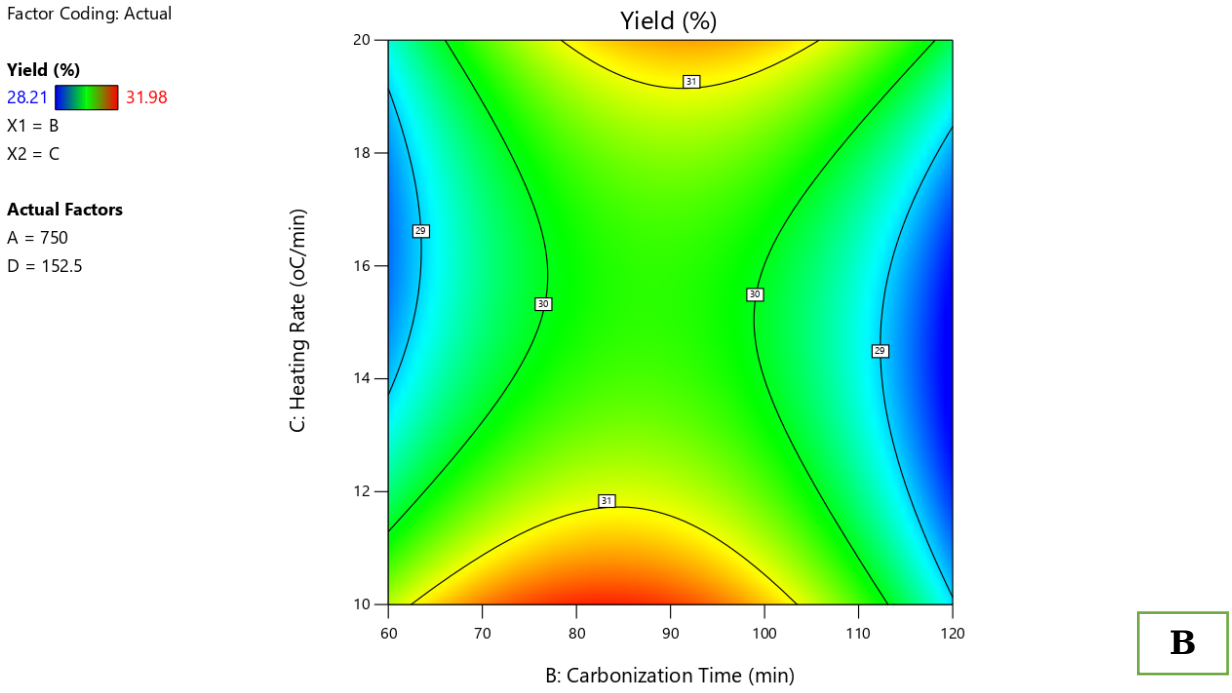

Figure 6. Interaction between Carbonization Time and Heating Rate on biochar yield: (A) 3D surface plot and (B) contour plot.

While the interaction between carbonization time and particle size (term BD, $p = 0.2986$) was not statistically significant, the trend shown in Figure 7 provides some qualitative insight. There appears to be a modest improvement in yield for smaller particles (125–150 µm) with extended carbonization times, possibly due to better heat transfer and more complete volatile release [74]. However, the insignificant p-value suggests that, within the experimental range tested, this interaction did not contribute meaningfully to the predictive power of the model. The relatively uniform surface also indicates that these factors act more independently rather than synergistically in influencing biochar yield.

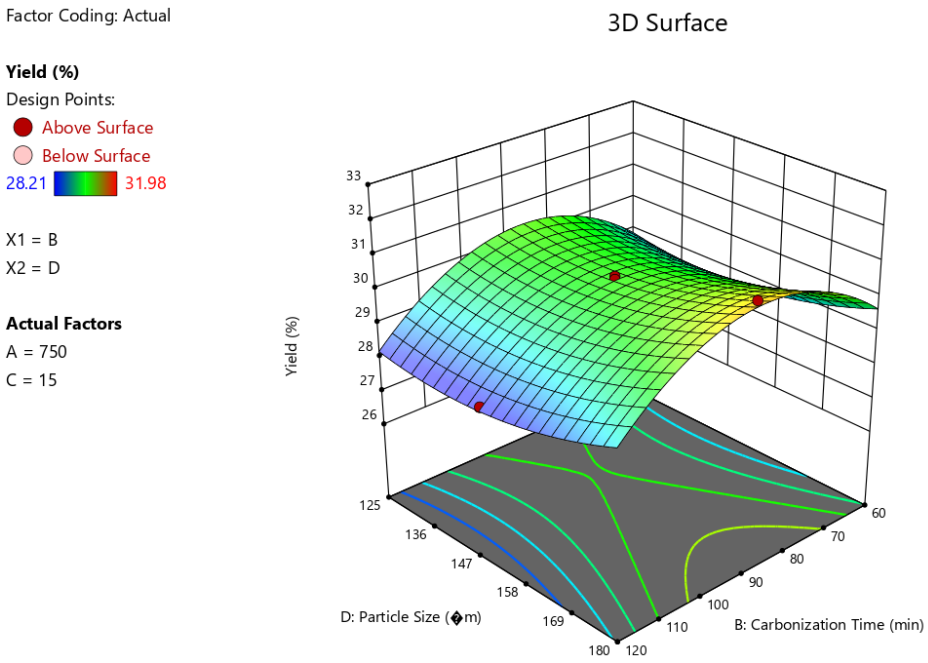

A

455

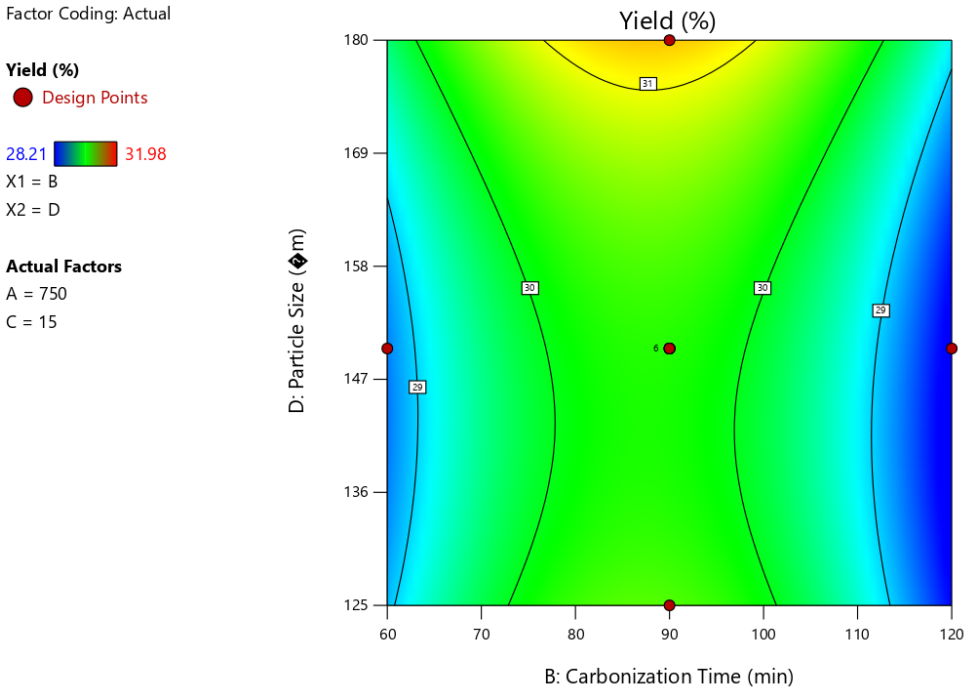

B

456

457 Figure 7. Interaction between Carbonization Time and Particle Size on biochar yield: (A) 3D

458 surface plot and (B) contour plot.

The interaction term between heating rate and particle size (CD, $p = 0.1434$) was statistically insignificant; however, the response surface in Figure 8 revealed meaningful variation in yield across the factor space. Notably, higher biochar yields were observed at both extremes of particle size, particularly under low heating rate conditions. At low heating rates (~10 °C/min), both fine (125 µm) and coarse (180 µm) particles resulted in improved yield, likely due to enhanced thermal stability and more gradual pyrolysis. Additionally, high heating rate combined with large particle size also led to elevated yield, possibly because the larger biomass structure prevented excessive tar formation or structural collapse [68]. In contrast, the combination of fine particle size and high heating rate resulted in the lowest yield region (yellow zone), likely due to rapid devolatilization and volatile loss, where fast heating of fine particles promotes excessive tar formation or reduced carbon retention before stable char can form [75]. Despite the lack of statistical significance, the observed trends support known thermal decomposition behavior where heat transfer uniformity and particle mass play key roles in determining solid product retention.

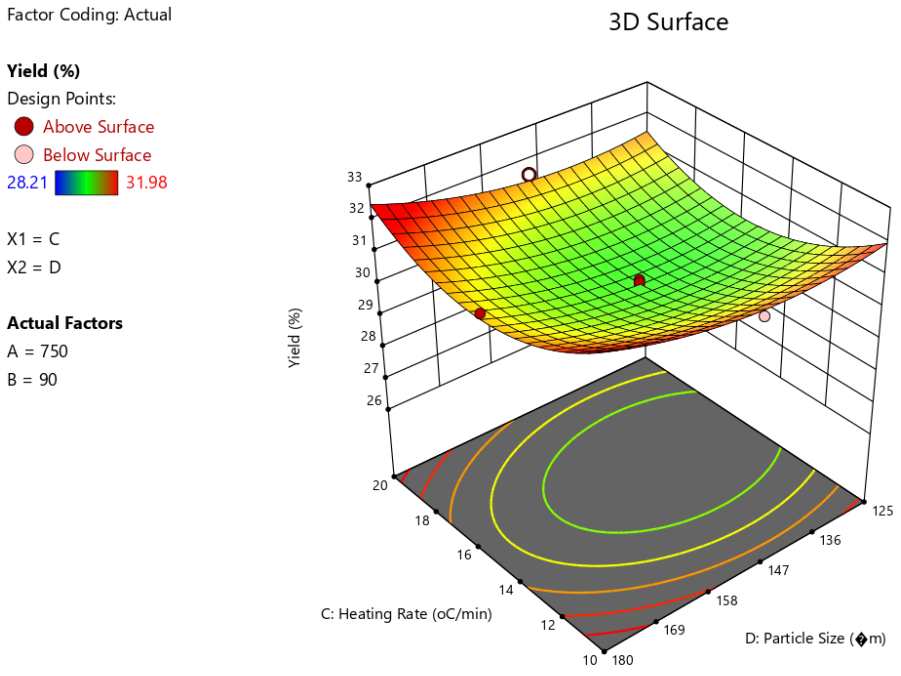

A

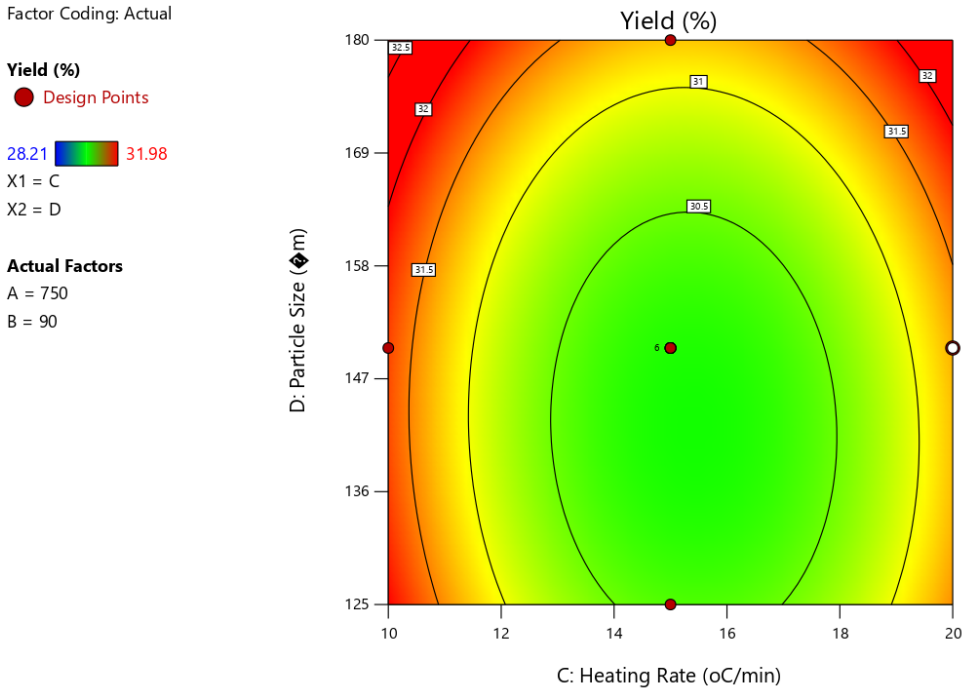

B

Figure 8. Interaction between Heating Rate and Particle Size on biochar yield: (A) 3D surface plot and (B) contour plot.

3.4. Process optimization for yield

Numerical optimization was performed using the response surface methodology (RSM) to maximize biochar yield while maintaining feasible processing conditions. The optimization criteria were set to minimize carbonization temperature, carbonization time, and heating rate, while maximizing particle size and yield. Out of 92 generated solutions, the most desirable set of parameters was identified as: carbonization temperature of 600 °C, carbonization time of 62.694 minutes, heating rate of 10 °C/min, and particle size of 179.996 µm, which collectively yielded a maximum predicted biochar yield of 31.98% with an overall desirability of 0.991.

This optimal point is visually supported by the ramps plot (Figure 9A), which clearly illustrates how each factor contributes to achieving the optimal yield within the defined boundaries. All input variables converge near their respective extremes, highlighting the

sensitivity of biochar synthesis to these critical process parameters. Additionally, the desirability overlay plot (Figure 9B) affirms the robustness of the optimization, with individual desirability values approaching unity: carbonization temperature (0.999998), carbonization time (0.955092), heating rate (0.999999), particle size (0.999926), and yield (1.000000). These high individual scores indicate strong agreement between model prediction and optimization goals, confirming that the selected conditions offer both operational feasibility and superior yield potential. Taken together, these results validate the model's utility for guiding scalable, high-yield biochar production under optimized thermal and physical conditions.

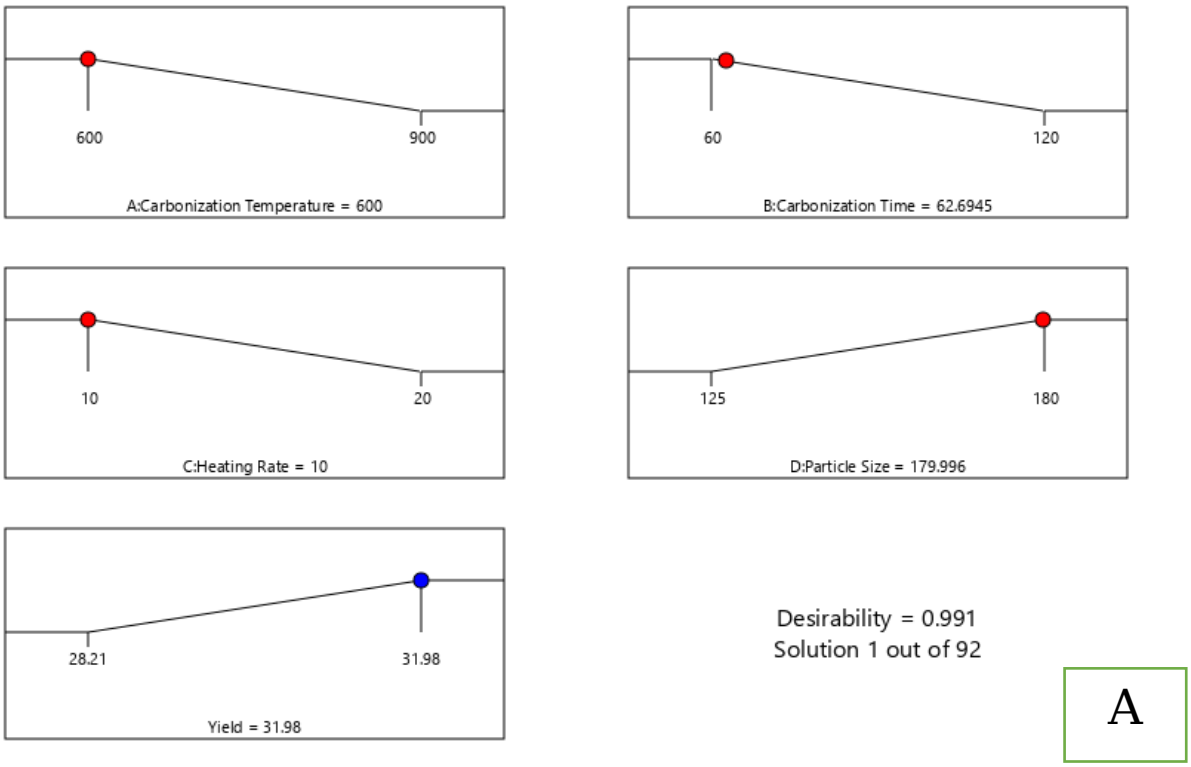

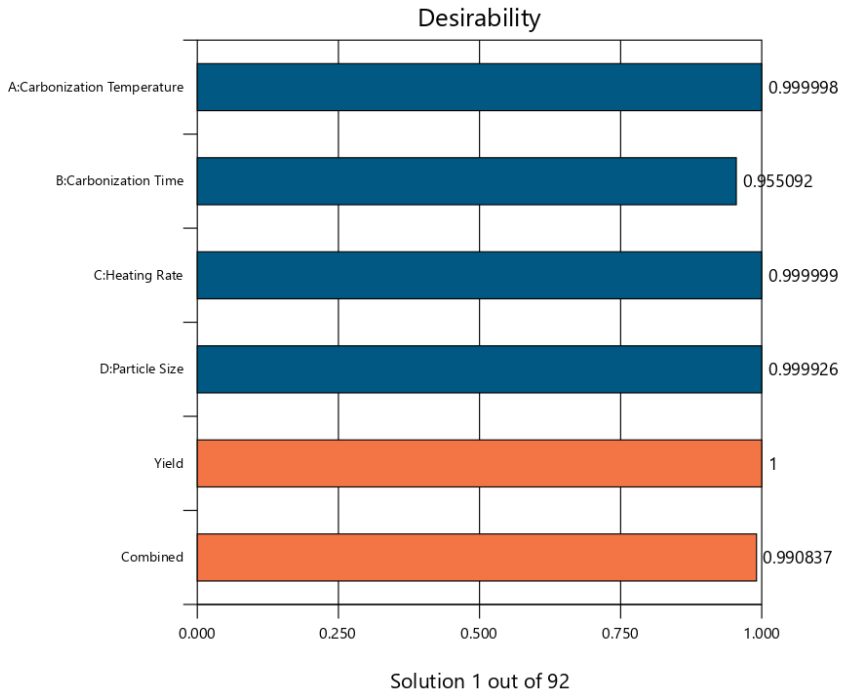

B

Figure 9. Optimization plots for biochar yield: (A) Ramps plot showing optimal conditions for each process variable contributing to maximum yield, and (B) Desirability overlay plot indicating high desirability scores for all factors, with an overall desirability

3.5. The Effect of Individual Factors on Biochar Yield

Biochar yield exhibited a decreasing trend with increasing carbonization temperature across the tested range (600–900 °C). The maximum yield of 30.96% was observed at 600 °C, followed by a steady decline to 29.72% at 900 °C. This monotonic decrease suggests a negative linear relationship between temperature and solid yield under fixed time, heating rate, and particle size conditions (90 min, 15 °C/min, 150 µm). Although temperature showed a strong effect, as confirmed by its highly significant p-value in the ANOVA table ($p < 0.0001$), the overall variation was relatively narrow (only ~1.24 percentage points across the full range). This indicates that temperature, while impactful, caused more subtle changes in solid recovery compared to other factors. The trend is visually captured in Figure 10.

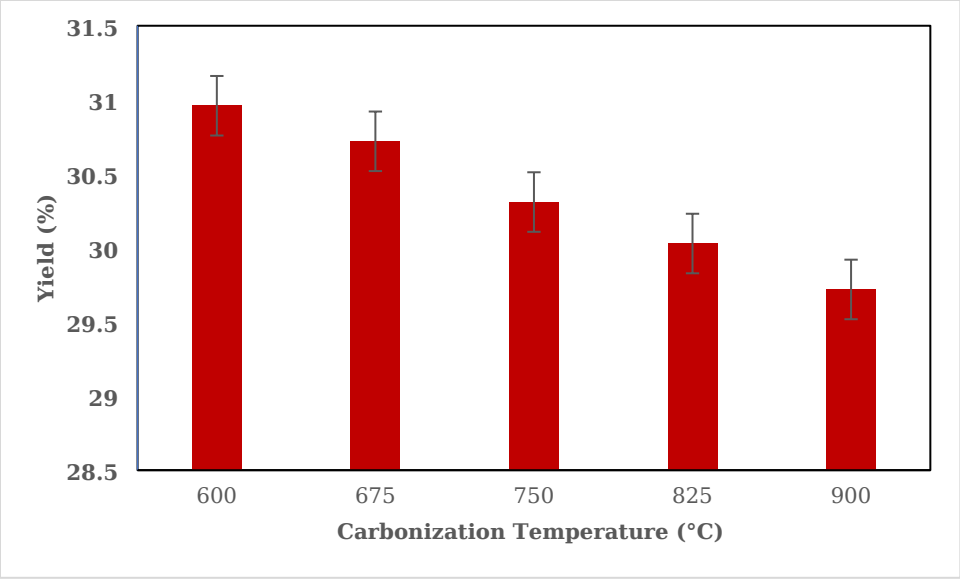

Figure 10. Effect of Carbonization Temperature on Biochar Yield

While the individual factor analysis revealed a monotonic decrease in biochar yield with increasing temperature (Figure 10), the interaction plots in Section 3.3.1 and 3.3.2 indicated that yield can initially improve with temperature when paired with specific levels of carbonization time or heating rate. This reinforces that temperature's influence is not purely independent but is shaped by its synergistic behavior with other process parameters.

As illustrated in Figure 11, yield initially increased with carbonization time from 60 to 90 minutes (from 28.72% to 30.26%) and then declined to 28.11% at 120 minutes. This non-linear, bell-shaped trend suggests that 90 minutes is an optimal point for maximizing biochar retention. The total variation across the range (~2.15%) is more pronounced than that observed for temperature, and ANOVA results confirm the statistical significance of time ($p < 0.0001$). The sharp decline at longer durations highlights the importance of controlling residence time to avoid excessive devolatilization or carbon loss. Although similar dynamics were discussed in the interaction section, this univariate profile reinforces that carbonization time is a critical tuning parameter even when other factors are held constant.

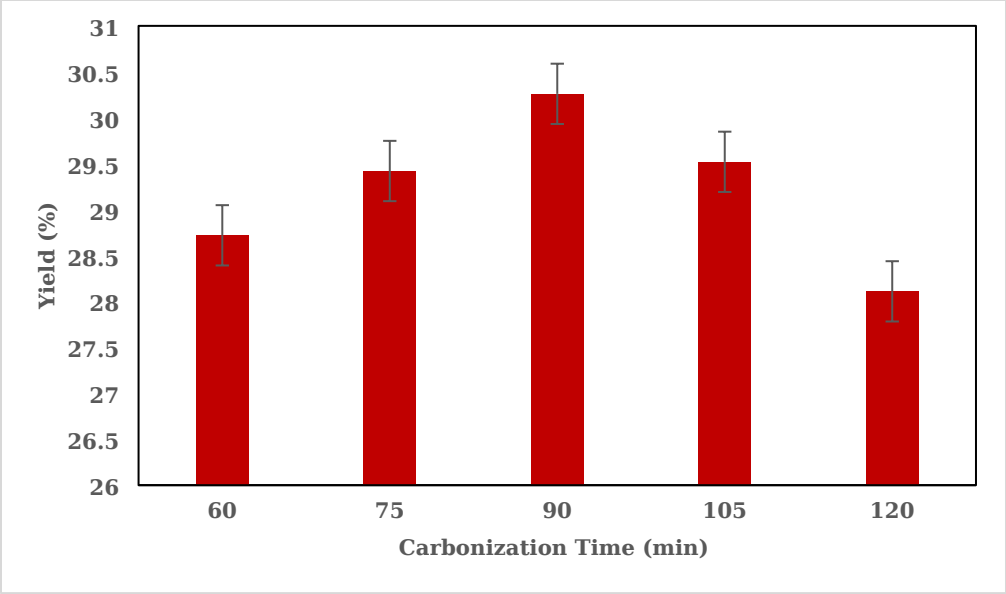

Figure 11. Effect of Carbonization Time on Biochar Yield

In contrast to the smooth, bell-shaped trend seen under fixed conditions in Figure 11, interaction effects (particularly with temperature and heating rate in Sections 3.3.1 and 3.3.4) showed sharper peaks or valleys in biochar yield depending on the specific combinations. This reflects that the effectiveness of residence time is context-dependent, varying with the rate of heat exposure and thermal severity.

The effect of heating rate on biochar yield, presented in Figure 12, was more complex than a linear trend. The yield peaked at the lowest level (10 °C/min) with 31.75%, declined to 30.34% at 15 °C/min, and then rose slightly again to 31.37% at 20 °C/min. This irregular pattern indicates that the heating rate had a relatively weaker and less predictable influence when other parameters were fixed (750 °C, 90 min, 150 µm). Despite its statistical significance in the ANOVA table ($p = 0.0004$), the range of variation (about 1.41%) was narrower than that observed for carbonization time or particle size.

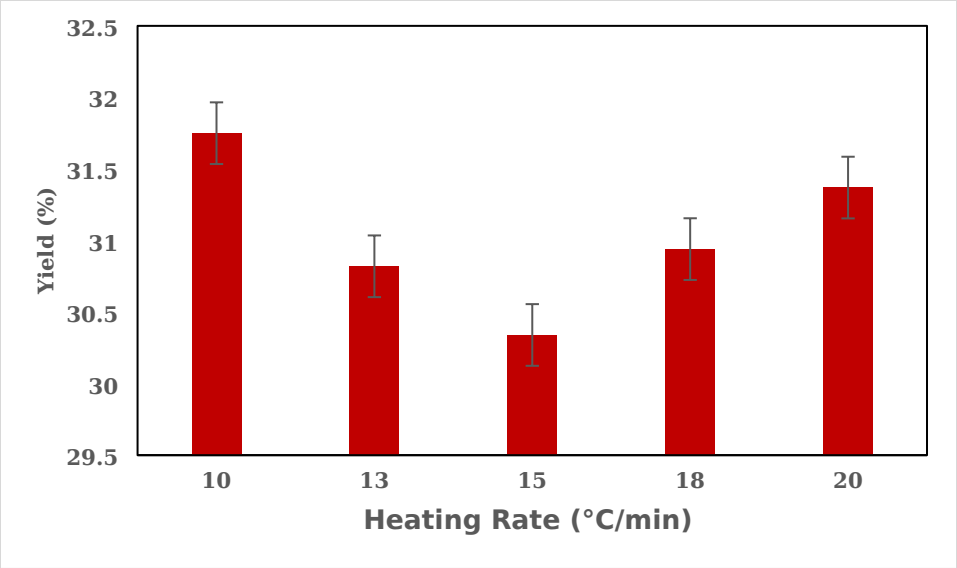

Figure 12. Effect of Heating Rate on Biochar Yield

Although heating rate showed a relatively weak and inconsistent trend in the individual factor plot (Figure 12), its impact was much more pronounced when interacting with temperature and carbonization time (Sections 3.3.2 and 3.3.4), where even small changes in rate significantly influenced the pyrolysis dynamics. This suggests that heating rate plays a more interactive role, modulating thermal gradients and mass transfer depending on surrounding conditions.

The effect of particle size on yield, depicted in Figure 13, showed a consistent increasing trend across the range of 106–212 µm. Yield rose from 30.04% at the finest size (106 µm) to 31.42% at the coarsest (212 µm), indicating a direct, positive linear effect. The variation (~1.38%) was moderate, and the trend was clear, supporting particle size as a meaningful individual contributor. The statistical analysis ($p < 0.0001$) further confirms its influence. Unlike time and temperature, where peak values occurred at intermediate levels, particle size exhibited no sign of an optimum within the tested range, suggesting that even larger sizes may further enhance char retention.

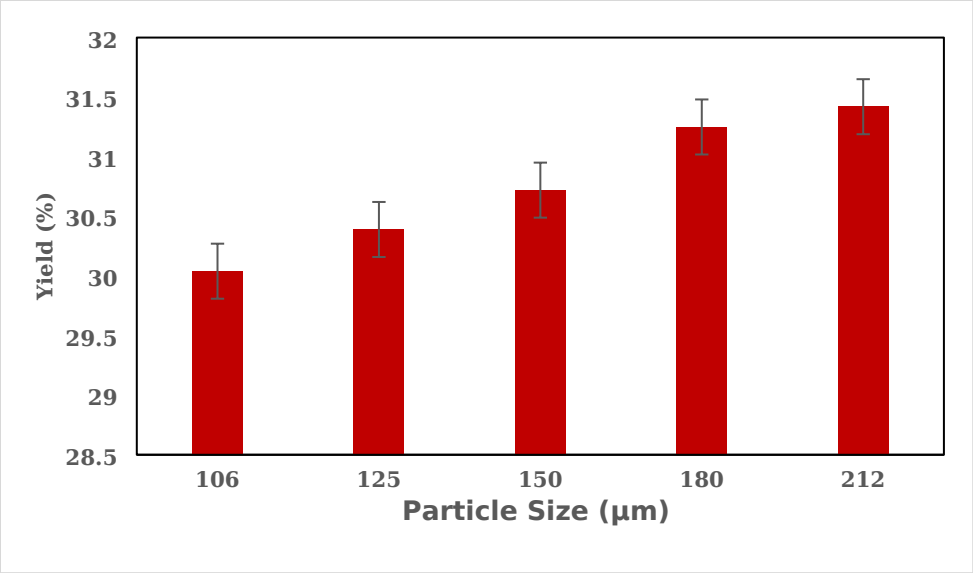

Figure 13. Effect of Particle Size on Biochar Yield

Interestingly, particle size showed a direct and consistent increase in yield under fixed conditions (Figure 13), yet its interaction with temperature and heating rate (Sections 3.3.3 and 3.3.6) revealed that finer particles often improved yield due to better thermal uniformity and faster volatile release. This contrast underscores the importance of considering interaction effects before drawing general conclusions from univariate trends.

3.6. Characteristics of Optimized Biochar

3.6.1. Proximate Analysis

Proximate analysis of the synthesized biochar was performed to determine its moisture content (MC), volatile matter (VM), ash content (AC), and fixed carbon (FC). These parameters provide insights into the thermal stability and quality of the biochar for soil amendment applications. The results are presented in Table 6.

Table 6. Proximate composition of biochar synthesized in this study compared with values reported in previous literature

Feedstock	MC (%)	VM (%)	AC (%)	FC (%)	Reference
Rumex abyssinicus	3.6	12.8	4.8	78.8	This study
Chlorella Pyrenoidosa Microalgae	1.9	31.62	12.18	54.3	[76]
Chlorella Vulgaris	3.81	17.4	13.45	65.34	[77]
Jatropha Seed	2.3	36.4	12.8	48.5	[78]
Mahua	5.14	36.17	8.66	50.03	[79]
Rice Husk	4.8	16.8	23.1	55.2	[80]
Oil Palm Fronds	5.7	19.9	2.4	72	[81]

The biochar exhibited low moisture (3.6%) and ash content (4.8%), indicating high thermal resistance and minimal inorganic residue, which are desirable for soil application [82]. The volatile matter content of the biochar was found to be 12.8%, which falls within the expected range for biomass pyrolyzed at 600 °C. This value reflects a moderate presence of labile organic compounds, suggesting that the biochar retains some capacity to stimulate microbial activity and enhance short-term nutrient cycling when applied to soil [83]. Compared to higher-VM biochars such as *Jatropha seed* (36.4%) or *Mahua* (36.17%), the lower VM in *Rumex abyssinicus* biochar implies a more thermally stable material with better resistance to biological degradation over time.

The most notable feature of the biochar was its high fixed carbon content, measured at 78.8%. This value exceeds that of many biochars in the literature, including those derived from *Chlorella vulgaris* (65.34%), *oil palm fronds* (72.0%), and *rice husk* (55.2%). High fixed carbon reflects a greater degree of carbonization and a higher potential for long-term carbon

sequestration in soils [84]. It also contributes to the structural stability of the biochar, enhancing its ability to persist in the environment and act as a long-lasting soil amendment [85].

3.6.2. Elemental Analysis

The elemental composition of the biochar was estimated using empirical correlations developed in [30], which provides valuable insight into its role as a soil amendment for rehabilitating degraded soils. Based on the proximate analysis results, the calculated carbon, hydrogen, and oxygen contents were approximately 43.92 wt%**,** 5.53 wt%**,** and 41.20 wt%**,** respectively, while nitrogen was estimated at 4.55 wt%**.** The moderate carbon content suggests a significant presence of both aromatic and less-condensed carbon structures, indicative of biochars produced at intermediate pyrolysis temperatures, which can contribute to both medium-term carbon sequestration and soil structural improvement [86] . Carbon-rich biochars such as this promote soil aggregate formation, enhance water retention, and reduce bulk density, key factors for restoring physically degraded soils [87]. The hydrogen content, while moderate, reflects a balance between aliphatic and aromatic compounds, supporting the biochar's physicochemical reactivity and interaction potential within the soil matrix [88]. The substantial oxygen content indicates the presence of polar functional groups, such as carboxyl and hydroxyl moieties, which enhance cation exchange capacity, improve nutrient retention, and mediate interactions with soil colloids and microbial communities [89]. Notably, the nitrogen content, higher than initially expected, suggests potential nutrient contribution, especially when biochar is used alongside other organic or inorganic soil amendments [87]. Collectively, this elemental profile supports the biochar's multifunctionality: acting as a physical and chemical soil conditioner while influencing biogeochemical cycling in degraded soils.

3.6.3. X-ray Fluorescence (XRF) Analysis

The elemental composition of the biochar derived from *Rumex abyssinicus* was determined by X-ray fluorescence (XRF) analysis. The results were converted into their corresponding

oxide forms to better represent the mineralogical profile and assess the biochar's chemical reactivity (Table 7).

Table 7. XRF Analysis of Elemental and Oxide Composition of *Rumex abyssinicus* Biochar

Element	Elemental Concentration (%)	Oxide Form	Oxide Concentration (%)
K	17.31	K_2O	41.71
Ca	9.31	CaO	13.03
Cl	4.81	Cl_2O	11.80
Si	1.57	SiO_2	3.36
P	1.15	P_2O_5	5.27
Fe	0.65	Fe_2O_3	1.86
Ti	0.59	TiO_2	0.99
Mn	0.13	MnO_2	0.20
V	0.31	V_2O_5	1.11
Mo	0.066	MoO_3	0.099
Al	0.51	Al_2O_3	1.93
Pb	0.014	PbO	0.015
Zn	0.020	ZnO	0.025
Nb	0.17	Nb_2O_5	0.49
Sr	0.029	SrO	0.034
Zr	0.041	ZrO_2	0.055
Rb	0.004	Rb_2O	0.008
U	0.006	U_3O_8	0.010

Biochar exhibited a mineral-rich composition dominated by potassium oxide (K_2O, 41.71%), calcium oxide (CaO, 13.03%), and chlorine oxide (Cl_2O, 11.80%). These elements contribute significantly to the biochar's alkalinity, which may aid in modifying soil pH and enhancing nutrient availability. The high potassium and calcium contents indicate the biochar's potential for improving soil fertility and nutrient stabilization [90].

Silica (SiO_2, 3.36%) and titanium dioxide (TiO_2, 0.99%) presence highlights the biochar's mineral framework. Silica enhances soil physical properties such as aeration and water retention, while titanium dioxide may confer photocatalytic properties, beneficial for degradation of organic contaminants and metal adsorption [91,92].

Trace metal oxides like iron oxide (Fe_2O_3, 1.86%) and manganese dioxide (MnO_2, 0.20%) suggest catalytic potential for redox reactions, relevant for pollutant immobilization and degradation in soil remediation contexts [93]. Other micronutrients detected, including phosphorus pentoxide (P_2O_5, 5.27%), molybdenum trioxide (MoO_3, 0.099%), vanadium

pentoxide (V_2O_5, 1.11%), and zinc oxide (ZnO, 0.025%), indicate biochar's role in supporting microbial activity and plant nutrient cycles [94,95]. Low levels of potentially toxic elements such as lead oxide (PbO, 0.015%) and uranium oxide (U_3O_8, 0.010%) warrant further safety evaluation before extensive agricultural use, although their concentrations are minimal [96].

3.6.4. Scanning Electron Microscope (SEM)

The SEM micrographs of the produced biochar reveal a highly porous microstructure characterized by numerous irregularly shaped dark regions, which correspond to pores of varying sizes, some relatively large (Figure 14). This pronounced porosity is indicative of a substantial internal surface area, a critical attribute that enhances the biochar's capacity for water retention, nutrient adsorption, and microbial colonization [97].

The irregular pore morphology reflects the complex and heterogeneous nature of the biochar matrix, formed during pyrolysis under optimized conditions [98]. Such porous architecture facilitates improved interaction with soil particles when applied as an amendment, contributing to enhanced soil aeration and moisture dynamics.

This microstructural feature aligns with biochar's known ability to improve soil physical properties by providing additional pore spaces that mitigate compaction and increase aggregate stability. Consequently, the observed biochar porosity is expected to play a pivotal role in remediating degraded soils by promoting favorable conditions for root growth and microbial activity, thereby supporting soil fertility and resilience.

Figure 14. SEM image of the Biochar

3.6.5. Fourier Transform Infrared Spectroscopy (FTIR)

The FTIR spectrum of the biochar reveals a range of functional groups that contribute to its reactivity and suitability for soil amendment applications, as shown in Figure 15. The broad absorption band at 3621 cm^{-1} corresponds to O–H stretching vibrations, indicative of hydroxyl groups from phenolic structures or residual moisture [99]. The peak at 3027 cm^{-1} is associated with aromatic C–H stretching, while the band at 2001 cm^{-1} may reflect overtone or combination bands linked to conjugated systems or residual unsaturated structures. A prominent peak at 1550 cm^{-1} is attributed to aromatic C=C stretching, confirming the presence of thermally stable carbon frameworks [100]. Absorptions at 1383 cm^{-1} and 1261 cm^{-1} are assigned to C–H bending and C–O stretching, respectively, suggesting partial retention of oxygenated organic matter [101]. The strong band at 1117 cm^{-1} corresponds to C–O–C vibrations typical of ether linkages [102]. The peaks at 808 cm^{-1} and 617 cm^{-1} suggest out-of-plane bending of aromatic rings and possible metal–oxygen interactions [103]. These surface functionalities enhance the biochar's ability to retain nutrients, adsorb contaminants, and interact with soil microbiota, making it a promising candidate for restoring degraded soils. Similar FTIR profiles have been reported for biochars derived from lignocellulosic biomass, where oxygenated groups play a key role in improving soil fertility and water retention [104].

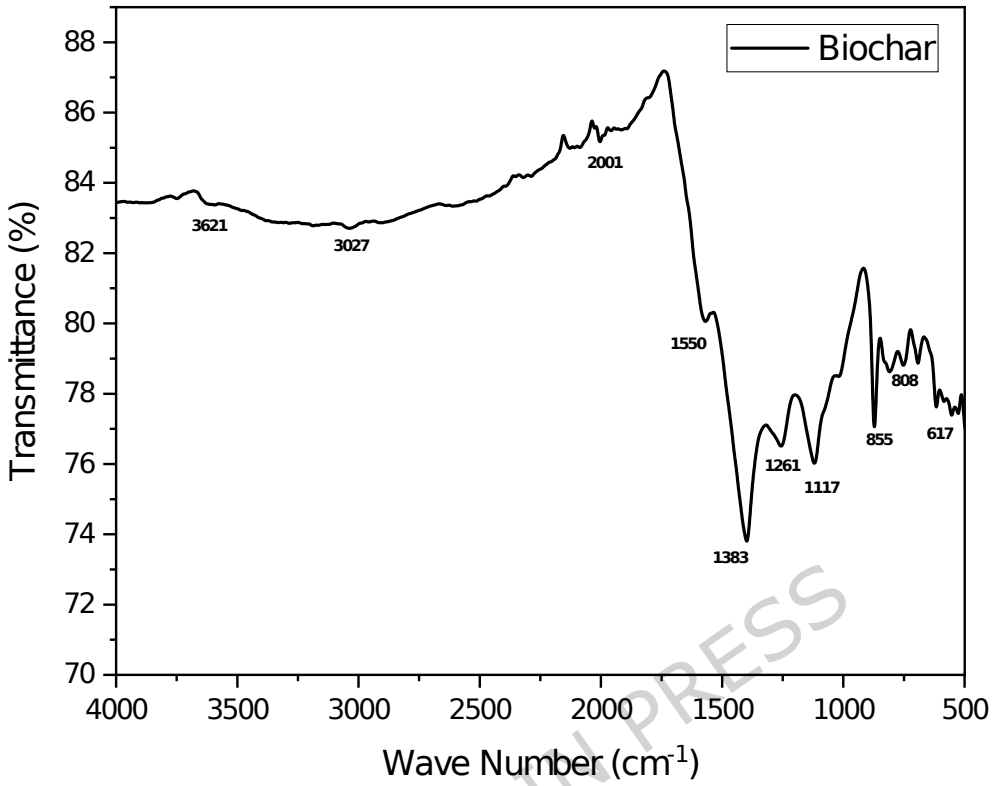

Figure 15. FTIR analysis of the Biochar

3.6.6. X-Ray Diffraction (XRD)

The X-ray diffraction (XRD) pattern of *Rumex abyssinicus* biochar, presented in Figure 16, reveals a predominantly amorphous structure with several low-intensity peaks scattered across the 2θ range. Compared to the biomass, the biochar shows broader and less defined reflections, indicating a loss of crystalline order due to thermal decomposition during pyrolysis. Notable peaks were observed at 21.36°, 24.68°, 28.28°, 29.4°, 30.32°, 33.36°, 40.58°, and 43.08°, suggesting the presence of residual mineral phases such as silica, aluminosilicates, or thermally stable oxides [105]. The absence of sharp graphitic peaks confirms that the carbon structure remains largely disordered, which is typical for biochar produced under moderate-to-high temperatures in inert atmospheres [106]. Using the Debye-Scherrer equation and the peak at 28.28°, the average crystallite size was estimated to be approximately 23.6 nm, indicating the presence of nanocrystalline domains embedded within

687 the amorphous matrix. This amorphous nature enhances the material's surface reactivity and
688 porosity, contributing to its effectiveness in soil amendment applications by improving water
689 retention, nutrient adsorption, and microbial colonization. Similar XRD profiles have been
690 reported for rice straw–derived biochars used in soil remediation, where increased pyrolysis
691 temperature led to reduced crystallinity and enhanced carbon sequestration potential [107].

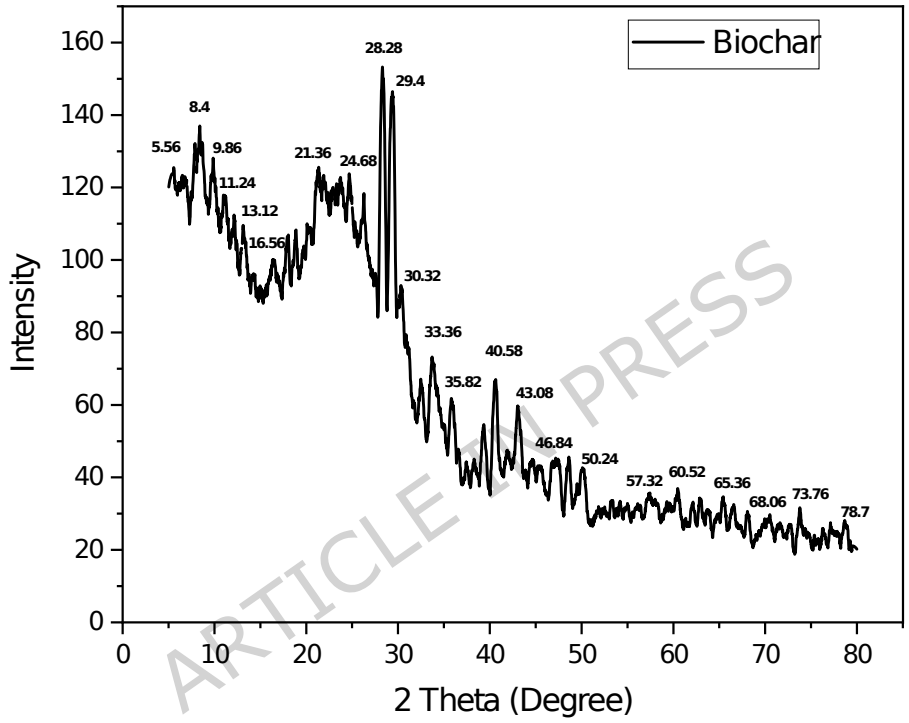

692

693 Figure 16. XRD analysis of the Biochar

694 **3.6.7. Thermogravimetric Analysis (TGA)**

695 The thermogravimetric analysis of the biochar revealed a multi-stage decomposition profile
696 under a nitrogen atmosphere, as shown in Figure 17. The initial weight loss below 150 °C is
697 attributed to the evaporation of physically bound moisture and volatile organics [108]. A
698 pronounced degradation phase occurs between approximately 250 °C and 400 °C,
699 corresponding to the breakdown of hemicellulose and cellulose fractions, which are typical
700 in lignocellulosic biomass-derived biochars [109]. A second major weight loss event is observed

between 450 °C and 600 °C, likely associated with the decomposition of more thermally stable components such as lignin and residual carbon structures [110]. Beyond 600 °C, the curve stabilizes, indicating the formation of a carbon-rich matrix with high thermal resistance [111]. This residual mass fraction is critical for soil amendment applications, as it reflects the biochar's potential for long-term carbon sequestration and structural persistence in degraded soils. Similar thermal behavior has been reported for biochars derived from agricultural residues, where high-temperature stability correlates with enhanced sorption capacity and reduced leaching risk in soil systems [112].

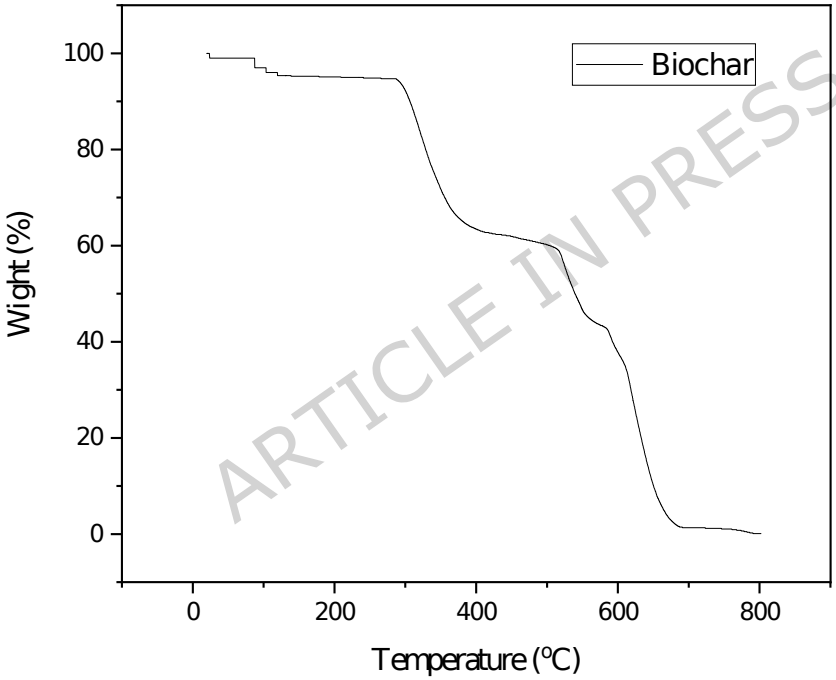

Figure 17. TGA graph of the Biochar

3.6.8. Brunauer-Emmett-Teller (BET) Surface Area Analysis

The BET surface area of the optimized biochar produced from *Rumex abyssinicus* was measured at 455.1 m^2/g, indicating the development of a well-structured porous matrix. While this value is notably higher than the 45.8 m^2/g reported by Teweldebrihan and Dinka [8] for *Rumex abyssinicus* biochar produced at 500 °C for 2 hours without chemical activation,

this discrepancy can be attributed to key differences in process parameters. In the present study, pyrolysis was conducted at a higher final temperature (600 °C), which is known to enhance pore development and surface area. Additionally, a slower heating rate (20 °C/min vs. 25 °C/min) and smaller feedstock particle size (180 µm vs. 250 µm) may have contributed to more effective thermal decomposition and pore formation. Although the residence time was the same (120 minutes), these combined factors likely account for the observed increase in surface area [8]. These thermal and physical variables are known to significantly influence the physicochemical characteristics of biochar, particularly pore formation [113]. Higher temperatures and longer residence times enhance devolatilization and the carbonization process, promoting the development of micro- and mesopores. Moreover, a smaller particle size facilitates more uniform heat distribution and greater surface reactivity during pyrolysis [114]. Although no chemical activation was applied, the observed surface area falls within the higher end of the range typically reported for thermally optimized lignocellulosic biochars (Table 8). This elevated surface area supports the potential of the material for soil remediation applications, as it enhances sorption capacity, improves nutrient and moisture retention, and promotes interactions with soil colloids. Additional characterization of pore volume and distribution would further elucidate the material's adsorption behavior.

Table 8. BET Surface Area Comparison of Biochar from This Study and Other Reported Biochars

Feedstock	**Carbonization Temperature (ºC)**	**Carbonization Time (min)**	**Heating Rate (ºC/min)**	**Particle Size (µm)**	**BET Surface Area (m^2/g)**	**Reference**
Rumex abyssinicus	600	120	20	180	455.1	This study
Rice husk	650	180	-	1000	261.72	[115]
Corn cob	800	120	1	-	17.03	[116]
Willow tree	700	-	-	-	840.6	[117]
Oak wood	800	120	10	-	231.15	[118]
Furfural residue	500	60	10	-	567	[119]
Rumex abyssinicus	500	180	25	250	45.8	[8]

Coconut shells	800	60	10	-	174.51	[120]
Broom and gorse wastes	600	180	3	2000	150	[121]

735

736 **3.6.9. Determination of Point of Zero Charge (pH_{PZC})**

737 The biochar produced from *Rumex abyssinicus* exhibited a point of zero charge (pHpzc) of
738 approximately 9.2, indicating that its surface carries a neutral net charge at this pH (Figure
739 18). At soil pH values below 9.2, typical of acidic degraded soils, the biochar surface becomes
740 positively charged. Conversely, at pH values above 9.2, the surface charge switches to
741 negative.

742 In acidic soils (pH < 7), despite the biochar surface also being positively charged, the
743 amendment effectively increases soil pH through its inherent alkaline properties rather than
744 purely electrostatic mechanisms [122]. The biochar's mineral ash content and alkaline
745 functional groups contribute to neutralizing excess H+ ions, thereby buffering soil acidity.
746 This chemical buffering is crucial for improving nutrient availability and microbial activity in
747 degraded soils [123].

748 Moreover, the porous biochar structure provides adsorption sites that can immobilize acidic
749 ions and heavy metals, enhancing soil remediation beyond simple charge interactions [124].
750 The pHpzc thus provides insight into the charge dynamics influencing nutrient retention and
751 soil chemistry, but the overall soil pH improvement is primarily driven by the biochar's
752 alkaline mineralogy and surface chemistry.

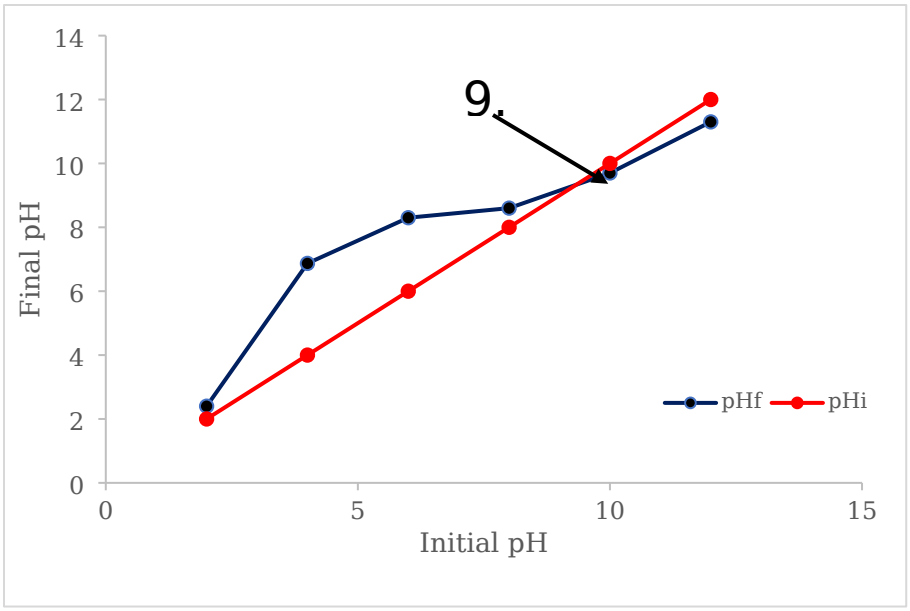

Figure 18. pHpzc of the Biochar

3.6.10. pH and Electric Conductivity

The synthesized *Rumex abyssinicus* biochar exhibited a moderately alkaline pH of 8.57, which is advantageous for remediating acidic or degraded soils by buffering acidity and enhancing nutrient availability [125]. Its electrical conductivity (EC) was measured at 1,010 µS/cm, indicating a moderate concentration of soluble salts. This EC level reflects the presence of essential mineral ions that can contribute to soil fertility, while remaining below salinity thresholds that typically pose agronomic risks, provided the biochar is applied at appropriate rates [126]. Guideline literature suggests that soils with EC below 4 dS/m (4,000 µS/cm) are generally considered non-saline and suitable for most crops [127], placing this biochar well within safe application limits.

3.4.11. Bulk Density, Particle Density, and Specific Gravity

The *Rumex abyssinicus* biochar exhibited a notably low bulk density of 0.095 g/cm³, which is significantly lower than the 0.136–0.185 g/cm³ range reported for agricultural residue biochars and the 0.12–0.17 g/cm³ range for pine and straw biochars [128,129]. This reduced density reflects its highly porous structure, likely resulting from the lignocellulosic composition of the biomass and the slow pyrolysis process used, which promotes extensive

pore development. While such low-density biochars can pose logistical challenges in terms of transport and field application due to their high volume-to-mass ratio, they offer agronomic advantages such as improved soil aeration, moisture retention, and microbial habitat. Additionally, their high porosity enhances surface area, potentially improving sorption capacity and long-term carbon sequestration in soils.

In contrast to its low bulk density, the *Rumex abyssinicus* biochar exhibited a particle density of 1.11 g/cm^3, which falls within the expected range for lignocellulosic biochars and is comparable to values reported for other biomass sources, such as giant reed (1.44–1.68 g/cm^3) [130]. Particle density represents the density of the solid material itself, excluding interparticle voids, and the value observed for *Rumex abyssinicus* indicates a well-developed carbon matrix with appreciable internal porosity. This density reflects a favorable balance between structural integrity and internal pore volume, suggesting the presence of predominantly amorphous carbon with moderate ash content. Such characteristics are advantageous for soil applications, as they promote enhanced water and nutrient retention, microbial colonization, and potential for long-term carbon sequestration without compromising material stability.

The specific gravity, matching the particle density at 1.11, confirms the material’s light solid-phase composition relative to water. As specific gravity is a dimensionless quantity, it serves as a comparative metric for understanding the biochar's potential interaction with water-based systems, including slurry formulations or soil moisture retention dynamics.

The large difference between bulk and particle density suggests that the biochar contains a very high proportion of void space, a key indicator of its total porosity. This highly porous architecture enhances the biochar's capacity for water retention, gas exchange, and the adsorption of nutrients or contaminants. These properties are particularly valuable in soil remediation, where the material must both physically improve soil structure and chemically interact with ions and organic compounds in the soil solution.

In practical terms, the combination of low bulk density, moderate particle density, and high internal porosity positions *Rumex abyssinicus* biochar as a promising amendment for improving soil physical properties in degraded or compacted landscapes. Its structure allows it to enhance aeration, reduce compaction, and support beneficial microbial habitats, while also enabling potential use as a carrier medium for nutrients, pesticides, or microbial inoculants in precision soil management strategies.

3.6.12. Water Holding Capacity (WHC), and Cation Exchange Capacity (CEC)

The *Rumex abyssinicus* biochar produced at 600 °C exhibited a water holding capacity (WHC) of 5.56 g water per gram of biochar, a value that underscores its substantial potential for enhancing soil moisture retention relative to other biomass-derived biochars at comparable pyrolysis temperatures. This WHC notably exceeds that of pine sawdust biochar (1.8 g/g at 600 °C) and hardwood biochar (~2.0–3.0 g/g at 500 °C) reported by Zhang et al. [131] and Suliman et al. [132], respectively, while aligning closely with oil palm fronds biochar (5.0–6.0 g/g at ~500 °C) as documented by Ahmad et al. [133]. The elevated WHC of *Rumex abyssinicus* biochar can be attributed primarily to its unique physical structure, characterized by its low bulk density (0.095 g/cm³) and particle density (1.11 g/cm³), which collectively signify a highly porous matrix with abundant micro- and mesopores. This porosity facilitates substantial internal void volume for water adsorption and retention, as well as enhanced surface area for hydrogen bonding with water molecules. Moreover, the low particle density indicates a predominance of amorphous carbon with hydrophilic functional groups that promote water affinity, further contributing to the observed WHC. The combination of these properties suggests that *Rumex abyssinicus* biochar possesses an optimal balance between porosity and surface chemistry, enabling it to retain water more effectively than many conventional biochars produced under similar thermal conditions. Consequently, this biochar represents a promising soil amendment for improving water availability in degraded or drought-prone soils, supporting microbial activity, and enhancing nutrient cycling. These attributes, coupled with the lightweight nature of the biochar, also

facilitate its field application and soil integration, offering practical advantages in sustainable land management and reclamation efforts.

The *Rumex abyssinicus* biochar produced at 600 °C exhibited a cation exchange capacity (CEC) of 15 meq/100g, placing it within the expected range for herbaceous biomass-derived biochars subjected to high-temperature pyrolysis. This value aligns with the lower end of the spectrum reported by Munera-Echeverri et al. [134], who documented CEC values ranging from 3.6 to 119.6 meq/100g depending on feedstock and extraction method, with herbaceous and low-ash biochars typically falling between 10 and 20 meq/100g. Compared to manure- and straw-based biochars, which often exceed 200 meq/100g due to their mineral-rich composition and lower pyrolysis temperatures [135], the moderate CEC of *Rumex* biochar reflects its condensed aromatic structure and relatively low ash content. Antonangelo et al. [136] further emphasized that biochar feedstock and ash content are critical determinants of CEC, noting that poultry litter biochar increased soil CEC by 91%, while switchgrass biochar reduced it by 27%. The 15 meq/100g CEC observed in this study suggests that *Rumex abyssinicus* biochar possesses sufficient exchangeable sites to enhance nutrient retention and reduce leaching in degraded soils, without the excessive ionic saturation that may disrupt microbial balance. This moderate CEC complements its high-water holding capacity, reinforcing its potential as a multifunctional amendment for soil restoration and sustainable land management.

3.7. Characteristics of Degraded Soil

The baseline physicochemical profile of the unamended soil (Table 9) reveals a system in clear decline, exhibiting multiple indicators of degradation as defined by FAO and global soil health frameworks. Bulk density (1.33 ± 0.04 g/cm^3) falls within the upper threshold for root proliferation, yet its proximity to compaction limits suggests restricted pore space and impaired aeration. Particle density (2.31 ± 0.04 g/cm^3) is notably lower than the mineral soil average, likely reflecting a depleted organic matrix and reduced structural integrity.

Porosity (42.47 ± 2.00%) sits at the lower bound for loamy soils, reinforcing the inference of poor aggregation. Critically, moisture content (6.10 ± 0.60%) and water holding capacity (17.80 ± 1.20%) are both suboptimal, confirming the soil's limited capacity to retain and supply water, an acute vulnerability under erratic rainfall regimes. The acidic pH (5.72 ± 0.12) further compounds nutrient stress, particularly phosphorus and micronutrient availability, while elevated exchangeable acidity (1.65 ± 0.08 meq/100g) signals potential aluminum toxicity, a known inhibitor of root elongation and microbial activity.

Nutrient dynamics are similarly constrained. Organic matter (1.45 ± 0.30%) is well below the 2% threshold for biologically active soils, and total Kjeldahl nitrogen (2650 ± 90 mg/kg) falls short of optimal fertility benchmarks. Cation exchange capacity (14.80 ± 0.60 meq/100g) is marginal, limiting the soil's ability to retain and buffer essential nutrients. Available potassium (21 ± 2 mg/kg) and calcium (36 ± 6 mg/kg) are critically low, undermining plant vigor and structural resilience. Although available phosphorus (74 ± 4 mg/kg) is within acceptable bounds, its bioavailability is likely compromised by the prevailing acidity.

The soil's texture, sandy loam with 63.16% sand and only 5.26% clay, further exacerbates its vulnerability. Coarse particles promote rapid drainage and nutrient leaching, while offering minimal support for microbial colonization or root anchorage. Taken together, these parameters reflect a system in ecological retreat: chemically imbalanced, physically fragile, and biologically impoverished.

Table 9. Physicochemical Properties of Degraded Soil

Parameter	Unit	Mean ± SD	FAO Standard Range
Bulk density	g/cm³	1.33 ± 0.04	1.1–1.6 (ideal: <1.4 for root growth)
Particle density	g/cm³	2.31 ± 0.04	2.60–2.65 is typical for mineral soils
Specific gravity	–	2.31 ± 0.04	-
Porosity	%	42.47 ± 2.00	40–60% for loamy soils
Moisture content	%	6.10 ± 0.60	10–25% typical for healthy topsoil
Water holding capacity (WHC)	%	17.80 ± 1.20	20–30% for loamy soils

pH		–	5.72 ± 0.12	6.0–7.5 optimal for most crops
Electrical conductivity (EC)		µS/cm	175.00 ± 18	<400 µS/cm = non-saline
Cation exchange capacity (CEC)		meq/100g	14.80 ± 0.60	>15 ideal for nutrient retention
Organic matter (OM)		%	1.45 ± 0.30	>2% preferred for healthy soils
Total Kjeldahl nitrogen (TKN)		mg/kg	2650 ± 90	>3000 preferred for fertile soils
Available phosphorus (P)		mg/kg	74 ± 4	15–100 depending on method
Available potassium (K)		mg/kg	21 ± 2	>50 preferred for cropping
Exchangeable acidity (H^+ + Al^{3+})		meq/100g	1.65 ± 0.08	<1.0 preferred
Exchangeable sodium (Na)		mg/kg	170 ± 35	<200 = non-sodic
Exchangeable calcium (Ca)		mg/kg	36 ± 6	>100 preferred for base saturation
Texture	Sand	%	63.16	
	Silt	%	31.58	
	Clay	%	5.26	
	USDA texture class	–	Sandy loam	

Because of these problems, the soil needs to be improved. Adding organic materials like biochar or compost can help fix the structure, hold more water, balance the pH, and bring back nutrients. If nothing is done, the soil will stay weak and will not support healthy crops or restore the land.

3.8. Soil Amendment Test

3.8.1. Pot Experiment

To evaluate the effect of biochar on degraded soil, a pot experiment was conducted using four amendment levels: 0%, 10%, 15%, and 20% biochar by weight. After 100 days of incubation, the soils were analyzed for key physicochemical properties. The results are presented in Table 10, and the experimental setup is shown in Figure 19. Biochar application led to clear improvements in soil structure and fertility. Bulk density decreased significantly with higher biochar rates, from 1.32 g/cm³ in the control to 0.67 g/cm³ at 20% biochar. This reduction is attributed to biochar's inherently low density and porous architecture, which dilutes the compact mineral fraction and enhances soil aeration [137]. Porosity increased from 26.78% to 48.61%, reflecting the expansion of pore space that facilitates water infiltration

and gas exchange [138]. Moisture content and water holding capacity (WHC) improved markedly, rising from 6.34% to 12.40% and from 18.15% to 36.23%, respectively. These enhancements are due to biochar's high surface area and internal pore structure, which act as reservoirs for water retention [40].

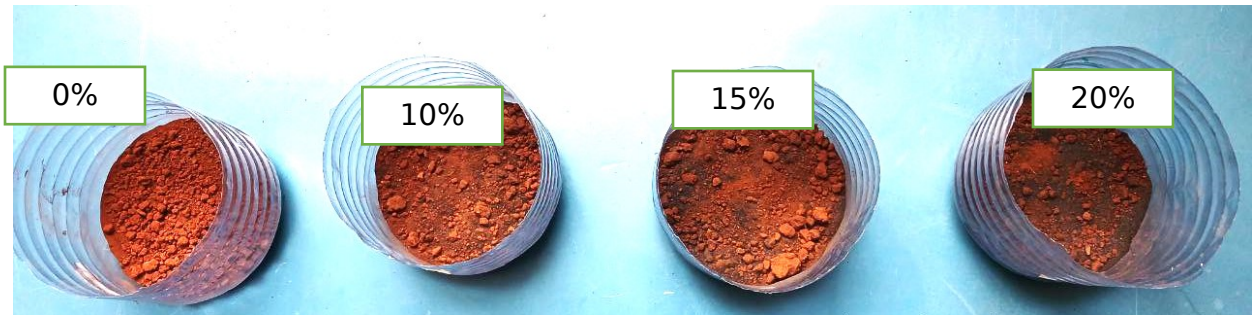

Figure 19. Pot experiment showing biochar-amended soils at 0%, 10%, 15%, and 20% application rates

The increase in pH from 5.78 to 7.20 indicates a shift from acidic to near-neutral conditions, which improves nutrient availability and reduces aluminum toxicity, a common issue in degraded tropical soils [139]. Electrical conductivity (EC) increased with biochar application, reaching 320.43 µS/cm at the highest rate. While this rise reflects improved mineral availability, the values remained well within agronomic safety thresholds, indicating no salinity risk under the tested conditions [140]. Cation exchange capacity (CEC) increased modestly from 15.00 to 17.00 meq/100g, reflecting the contribution of surface functional groups and ash minerals in biochar that enhance nutrient retention [141].

Organic matter (OM) content increased substantially from 1.50% to 6.47%, consistent with biochar's carbon-rich composition and its role in long-term carbon sequestration [142]. Total Kjeldahl nitrogen (TKN) increased from 2700 to 3000 mg/kg, likely due to nitrogen adsorption on biochar surfaces and reduced leaching losses [143]. Available phosphorus (P) and potassium (K) showed moderate gains, attributed to biochar's mineral content and its ability to reduce nutrient fixation in acidic soils [144]. Exchangeable acidity ($H^+ + Al^{3+}$) declined from 1.60 to 1.30 meq/100g, indicating reduced toxic ion concentrations and improved soil

buffering capacity [145]. Sodium (Na) and calcium (Ca) levels increased, contributing to better nutrient balance and flocculation of clay particles, which enhances soil structure [55,146]. Importantly, soil texture remained unchanged across treatments, with all samples retaining a sandy loam classification. This confirms that biochar did not alter the mineral fraction of the soil, but rather improved its functional properties [147]. These results demonstrate that biochar amendment significantly enhances the physical and chemical quality of degraded soil.

Table 10. Effect of Biochar Amendment on Physicochemical Properties of Degraded Soil (Mean ± SD, n = 3)

Parameter	**Unit**	**0% BC Amended Soil**	**10% BC Amended Soil**	**15% BC Amended Soil**	**20% BC Amended Soil**
Bulk Density	g/cm³	1.32 ± 0.03	0.95 ± 0.04	0.58 ± 0.02	0.67 ± 0.03
Particle Density	g/cm³	2.30 ± 0.05	2.10 ± 0.05	1.80 ± 0.04	1.95 ± 0.05
Porosity	%	26.78 ± 1.5	34.67 ± 2.0	41.48 ± 2.2	48.61 ± 2.5
Moisture Content	%	6.34 ± 0.7	8.50 ± 0.9	10.50 ± 1.0	12.40 ± 1.2
Water Holding Capacity (WHC)	%	18.15 ± 1.2	24.67 ± 1.5	30.53 ± 1.8	36.23 ± 2.0
pH	–	5.78 ± 0.10	6.30 ± 0.10	6.75 ± 0.12	7.20 ± 0.15
Electrical Conductivity (EC)	µS/cm	180.34 ± 15	240.65 ± 20	310.40 ± 25	320.43 ± 25
Cation Exchange Capacity (CEC)	meq/100g	15.00 ± 0.5	16.00 ± 0.6	16.50 ± 0.6	17.00 ± 0.7
Organic Matter (OM)	%	1.50 ± 0.3	4.16 ± 0.5	5.43 ± 0.6	6.47 ± 0.7
Total Kjeldahl Nitrogen (TKN)	mg/kg	2700 ± 80	2800 ± 90	2900 ± 90	3000 ± 100
Available Phosphorus (P)	mg/kg	76 ± 3	81 ± 4	86 ± 4	94 ± 5
Available Potassium (K)	mg/kg	22 ± 1	23 ± 1	23.5 ± 1.2	24 ± 1.2
Exchangeable Acidity ($H^+ + Al^{3+}$)	meq/100g soil	1.60 ± 0.08	1.50 ± 0.08	1.40 ± 0.08	1.30 ± 0.08
Exchangeable Sodium (Na)	mg/kg	180 ± 30	210 ± 40	350 ± 50	450 ± 60
Exchangeable Calcium (Ca)	mg/kg	38 ± 5	50 ± 6	70 ± 7	90 ± 8
Texture	Sand (%)	63.16	63.16	63.16	63.16
	Silt (%)	31.58	31.58	31.58	31.58
	Clay (%)	5.26	5.26	5.26	5.26
	USDA Texture Class	Sandy loam	Sandy loam	Sandy loam	Sandy loam

The changes observed in Table 10 are consistent with findings from previous studies, as shown in Table 11, and support biochar's use as a sustainable strategy for soil restoration.

Table 11. Comparison of Biochar Effects on Soil Properties with Previous Studies

Parameter	% Change at 20% Biochar Amendment (This Study)	% Change (Other Study)	Reference
Bulk Density	-49.24%	-20.9%, -31%	148,149
Porosity	+81.47%	+41%, +64%	149,150
Moisture Content	+95.59%	+50%	151
WHC	+99.56%	+35.3, +18%	126,148
pH	+24.57%	+9.35%, +26.56%, +59%	55,151,152
EC	+110.91%	+40.8%	55
CEC	+13.33%	+45%,+77.45%, +428%, +54.15%	151–154
OM	+531.33%	+75.76%, +154.46%, +110.91%	152,154,155
TKN	+11.11%	+81.25%, +48.86%, + 284.6%%	152,154,156
Available Phosphorus (P)	+23.68%	+106.56%, +333%, +316.67%, +365.93%	55,152,154,155
Available Potassium (K)	+9.09%	+100.00%, +128.46%, +254.12%	152,154,155
Exchangeable Acidity	−18.75%	−75.33%, −94.21%	55,154
Exchangeable Sodium (Na)	+444.00%	+104.82%, +80.00%	154,155
Exchangeable Calcium (Ca)	+136.84%	+892%, +138.58%	154,155

Table 11 compares the results of this study with findings from previous research. The 49.24% drop in bulk density is higher than what other studies reported (−20.9% to −31%), likely because the biochar used here had very low density and high porosity, which helped loosen the soil. Porosity increased by 81.47%, also above the reported range (+41% to +64%), showing that biochar improved the soil's structure and air space. Moisture content and water holding capacity nearly doubled, confirming biochar's ability to retain water. The rise in pH (+24.57%) shows that biochar helped reduce soil acidity, which can improve nutrient availability. EC increased by 110.91%, but stayed within safe limits, meaning more minerals were available without causing salt stress. CEC rose slightly (+13.33%), less than in other studies, possibly due to the type of biochar used. OM increased by over 500%, showing strong carbon input from biochar. TKN, available phosphorus, and available potassium also increased, though less than in some reports, likely due to reduced leaching and better

nutrient retention. Exchangeable acidity dropped by 18.75%, helping reduce harmful ions like aluminum. Exchangeable sodium and Exchangeable calcium levels rose sharply, improving nutrient balance and soil structure. Overall, this study shows that biochar can improve degraded soil more effectively than many previous reports, especially in terms of physical structure and water retention.

The one-way ANOVA results revealed statistically significant differences ($p < 0.05$) across several soil parameters following biochar amendment, indicating that biochar application had a measurable impact on soil physicochemical properties. Bulk density and water holding capacity (WHC) showed strong treatment effects, with F-values of 7.31 and 6.11, respectively, confirming that biochar significantly reduced compaction while enhancing moisture retention. Similarly, particle density ($F = 6.51$), pH ($F = 6.70$), and cation exchange capacity (CEC; $F = 9.63$) exhibited significant shifts, reflecting improved soil structure and nutrient retention potential. Available phosphorus and potassium also increased markedly ($F = 7.13$ and $F = 24.77$), suggesting enhanced nutrient availability. Electrical conductivity (EC) approached significance ($F = 5.66$; $p = 0.0548$), indicating increased ionic activity without exceeding salinity thresholds. Organic matter and exchangeable acidity both showed significant changes ($F > 9.6$), while exchangeable sodium and calcium displayed moderate effects ($F = 5.23$ and $F = 5.17$, respectively), supporting the role of biochar in modifying base saturation. These findings collectively demonstrate that biochar amendments significantly influence key soil parameters, validating its potential as a multifunctional soil conditioner for degraded land restoration.

3.8.2. Microstructural Analysis of Soil Before and After Amendment

The SEM micrographs of the degraded soil before biochar amendment revealed a predominance of bright, dense areas with minimal visible porosity (Figure 20A). The extensive light-reflective regions suggest a compacted, low-porosity matrix, characterized by tightly packed soil particles with limited pore spaces. This microstructure is indicative of poor soil aeration and water infiltration capacity, often observed in physically degraded soils.

The scarcity of visible cracks or pores further confirms a lack of soil aggregation and structural heterogeneity, which can restrict root growth and microbial activity [157,158].

Following the amendment with optimized *Rumex abyssinicus* biochar, the SEM images showed a marked increase in the abundance and size of pore spaces, appearing as irregularly shaped dark areas within the soil matrix (Figure 20B). This development of heterogeneous and well-distributed porosity reflects a substantial improvement in soil microstructure. The biochar particles appear to have introduced new micro-pores and facilitated particle aggregation, leading to enhanced soil aeration and water-holding capacity [153].

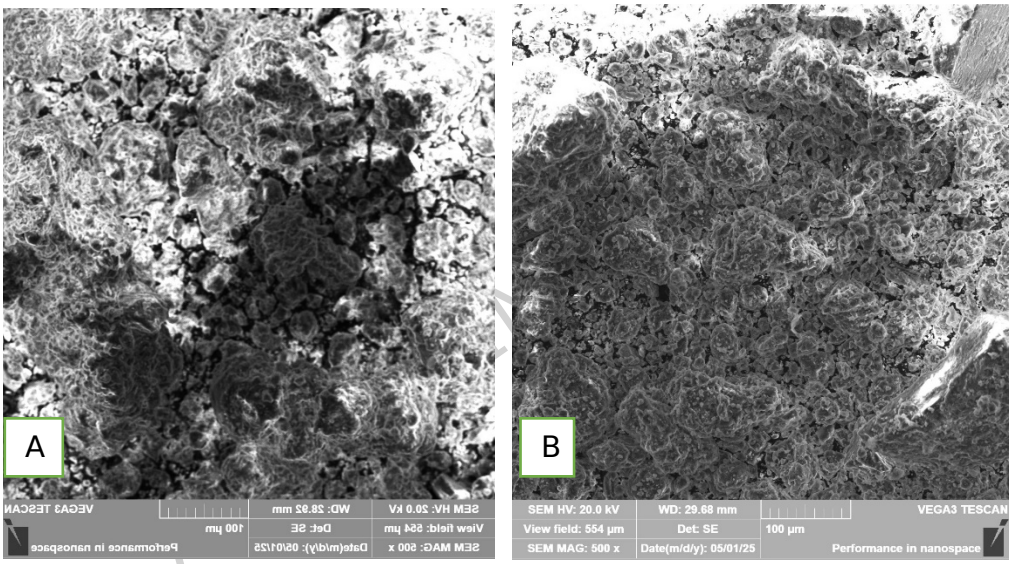

Figure 20. SEM image of soil before amendment (A), and after amendment (B)

The transition from a compacted, low-porosity soil to a more porous, aggregated structure suggests significant amelioration of physical soil properties due to biochar amendment. Increased porosity promotes improved water retention and drainage balance, creating a more favorable environment for root penetration and microbial colonization. These microstructural improvements are consistent with enhanced nutrient availability and soil respiration, which collectively support the restoration of degraded soils. The observed changes align with known biochar effects, where high surface area and porous morphology contribute to better soil aggregation and physicochemical stability.

4. Conclusion

This study provides the first comprehensive optimization and application of biochar derived from *Rumex abyssinicus* stems, addressing a critical gap in biochar research for Ethiopian agroecosystems. Using response surface methodology, pyrolysis conditions were fine-tuned to maximize yield and agronomic functionality, resulting in a biochar with high fixed carbon content, large surface area, and favorable chemical properties. Characterization confirmed its suitability for soil amendment, with strong water retention, moderate cation exchange capacity, and alkaline buffering potential.

Application of the optimized biochar to degraded soil from Wolayta led to statistically significant improvements in physical and chemical properties, including reduced bulk density, increased porosity, enhanced moisture retention, elevated pH, and improved nutrient availability. SEM analysis revealed substantial microstructural transformation, supporting the biochar's role in restoring soil aggregation and aeration.

Compared to previous studies, the biochar produced in this work demonstrated superior performance in physical soil rehabilitation, particularly in water holding capacity and organic matter enrichment. These results validate *Rumex abyssinicus* as a promising, locally sourced feedstock for biochar production and support its integration into sustainable land management strategies. The findings contribute to the development of scalable, climate-resilient soil amendment technologies tailored to Ethiopia's highland agroecology.

Data Availability

The data used to support the findings of this study are included in the article.

Conflicts of Interest

The authors declare that they have no conflicts of interest.

Authors' contribution

Writing – Review & Editing; Writing – Original Draft; Visualization; Validation; Methodology; Investigation; Formal analysis; Data curation; Conceptualization: S.T., A.W., T.G.W., and M.A. All authors have reviewed and approved the final version of the manuscript for publication.

Acknowledgments

We would like to thank Addis Ababa Science and Technology University for their technical assistance**.**

Funding Statement

Funding was not acquired for this study and only facilities were provided.

References

1. Mesele SA, Mechri M, Okon MA, et al. Current Problems Leading to Soil Degradation in Africa: Raising Awareness and Finding Potential Solutions. *Eur J Soil Sci*. 2025;76(1):e70069.

2. Tefera ML, Carletti A, Altea L, Rizzu M, Migheli Q, Seddaiu G. Land degradation and the upper hand of sustainable agricultural intensification in sub-Saharan Africa-A systematic review. *J Agric Rural Dev Trop Subtrop*. 2024;125(1):63-83.

3. Tadesse A, Hailu W. Causes and consequences of land degradation in Ethiopia: A review. *Int J Sci Qual Anal*. 2024;10(1):10-21.

4. Luo P, Zhang W, Xiao D, Hu J, Li N, Yang J. Biochar-Based Fertilizers: Advancements, Applications, and Future Directions in Sustainable Agriculture—A Review. *Agronomy*. 2025;15(5):1104.

5. Anyebe O, Sadiq FK, Manono BO, Matsika TA. Biochar characteristics and application: Effects on soil ecosystem services and nutrient dynamics for enhanced

crop yields. *Nitrogen*. 2025;6(2):31.

6. Shyam S, Ahmed S, Joshi SJ, Sarma H. Biochar as a Soil amendment: implications for soil health, carbon sequestration, and climate resilience. *Discov Soil*. 2025;2(1):18.

7. Yang J, Xia L, van Groenigen KJ, et al. Sustained benefits of long-term biochar application for food security and climate change mitigation. *Proc Natl Acad Sci*. 2025;122(33):e2509237122.

8. Teweldebrihan MD, Dinka MO. Methyl red adsorption from aqueous solution using Rumex Abyssinicus-derived biochar: Studies of kinetics and isotherm. *Water*. 2024;16(16):2237.

9. Yrga Adugna B, Mequanint Adinew G, Ayalew Getahun K, et al. Evaluation of the antidiabetic activity of hydromethanolic roots extracts of rumex abyssinicus jacq:(polygonaceae) in Swiss albino mice. *Evidence-Based Complement Altern Med*. 2022;2022(1):5193250.

10. Lemlemu A, Habtamu A, Atinafu G. Qualitative Phytochemical investigation of Rumex abyssinicus jacq root and Verbasicum sinaiticum Benth leaves. *Daagu Int J Basic Appl Res*. 2024;6(2):562-571.

11. Abewaa M, Mengistu A, Takele T, Fito J, Nkambule T. Adsorptive removal of malachite green dye from aqueous solution using Rumex abyssinicus derived activated carbon. *Sci Rep*. 2023;13(1):14701.

12. Fito J, Abewaa M, Mengistu A, et al. Adsorption of methylene blue from textile industrial wastewater using activated carbon developed from Rumex abyssinicus plant. *Sci Rep*. 2023;13(1):5427.

13. Tibebu S, Kassahun E, Ale TH, et al. The application of Rumex Abysinicus derived activated carbon/bentonite clay/graphene oxide/iron oxide nanocomposite for removal of chromium from aqueous solution. *Sci Rep*. 2024;14(1):19280.

14. Aboelela D, Saleh H, Attia AM, Elhenawy Y, Majozi T, Bassyouni M. Recent advances in biomass pyrolysis processes for bioenergy production: optimization of operating conditions. *Sustainability*. 2023;15(14):11238.

15. Onokwai AO, Okokpujie IP, Ajisegiri ESA, Oki M, Onokpite E, Babaremu K. Optimization of Pyrolysis Operating Parameters for Biochar Production from Palm Kernel Shell Using Response Surface Methodology. *Math Model Eng Probl*. 2023;10(3).

16. Bhattacharyya PN, Sandilya SP, Sarma B, et al. Biochar as soil amendment in climate-smart agriculture: opportunities, future prospects, and challenges. *J Soil Sci Plant Nutr*. 2024;24(1):135-158.

17. Singh J, Bhattu M, Liew RK, et al. Transforming rice straw waste into biochar for advanced water treatment and soil amendment applications. *Environ Technol Innov*. 2025;37:103932.

18. Guo F, Wang C, Wang S, Zhao X, Li G, Sun Z. The native SOC increase in woodland and lawn soil amended with biochar surpassed greenhouse—a seven-year field trial. *Sci Total Environ*. 2024;907:167924.

19. Fedeli R, Zhatkanbayeva Z, Loppi S. Soil amendment with biochar from slaughterhouse waste bones enhances soil quality and promotes the growth of crop plants. *Plant Biosyst Int J Deal with all Asp Plant Biol*. 2025;159(2):378-386.

20. Brown DR, Dettmann P, Rinaudo T, Tefera H, Tofu A. Poverty alleviation and environmental restoration using the clean development mechanism: a case study from Humbo, Ethiopia. *Environ Manage*. 2011;48:322-333.

21. Labiso TT, Yagaso ZS. Land suitability analysis for surface irrigation in Humbo woreda, wolaita zone, Southern Ethiopia: Land suitabilfile:///C:/Users/HP/Downloads/scholar - 2024-12-15T172559.665.risity

analysis. *EQA-International J Environ Qual*. 2021;44:32-43.

22. Abera D, Liben FM, Shimbir T, et al. Guideline for agronomy and soil fertility data collection in Ethiopia: national standard. Published online 2020.

23. Mele MA, Kumar R, Dada TK, Heydari A, Antunes E. Investigation of gold adsorption by ironbark biochar using response surface methodology and artificial neural network modelling. *J Clean Prod*. 2024;456:142317.

24. Remmani R, Yılmaz M, Benaoune S, Di Palma L. Optimized pyrolytic synthesis and physicochemical characterization of date palm seed biochar: unveiling a sustainable adsorbent for environmental remediation applications. *Environ Sci Pollut Res*. Published online 2024:1-15.

25. Ashebir H, Nure JF, Worku A, Msagati TAM. Prosopis juliflora biochar for adsorption of sulfamethoxazole and ciprofloxacin from pharmaceutical wastewater. *Desalin Water Treat*. 2024;320:100691.

26. Fonseca GC da, Oliveira MS, Martins CVC, de Souza JCP. How the carbonization time of sugarcane biomass affects the microstructure of biochar and the adsorption process? *Sustainability*. 2022;14(3):1571.

27. Ibrahheem M, Zidan A. The Effect of Integration Between Heat and Time Factors on the Efficiency of the Carbonization of Peanut Shells to Prepare Biochar. *SSRG, IJAES, v7*. 2020;(3).

28. Li X. Preparation and Adsorption Properties of Biochar/g-C3N4 Composites for Methylene Blue in Aqueous Solution. *J Nanomater*. 2019;2019(1):2394184.

29. Abdu M, Babaee S, Worku A, Msagati TAM, Nure JF. The development of Giant reed biochar for adsorption of Basic Blue 41 and Eriochrome Black T. azo dyes from wastewater. *Sci Rep*. 2024;14(1):18320.

30. Shen J, Zhu S, Liu X, Zhang H, Tan J. The prediction of elemental composition of

biomass based on proximate analysis. *Energy Convers Manag*. 2010;51(5):983-987.

31. Morales LF, Herrera K, López JE, Saldarriaga JF. Use of biochar from rice husk pyrolysis: assessment of reactivity in lime pastes. *Heliyon*. 2021;7(11).

32. Tibebu S, Kassahun E, Worku A, et al. Cr (VI) removal from aqueous solutions using Cordia Africana-based activated carbon/red clay/magnetite nanocomposite: optimization via one factor at a time and response surface methodology. *Biomass Convers Biorefinery*. Published online 2025:1-27.

33. Fito J, Tibebu S, Nkambule TTI. Optimization of Cr (VI) removal from aqueous solution with activated carbon derived from Eichhornia crassipes under response surface methodology. *BMC Chem*. 2023;17(1):4.

34. Worku Z, Tibebu S, Nure JF, et al. Adsorption of chromium from electroplating wastewater using activated carbon developed from water hyacinth. *BMC Chem*. 2023;17(1):85.

35. Călin C, Sîrbu EE, Tănase M, György R, Popovici DR, Banu I. A Thermogravimetric Analysis of Biomass Conversion to Biochar: Experimental and Kinetic Modeling. *Appl Sci*. 2024;14(21):9856.

36. Zhang Y, Xia Z, Nafsun AI, Feng W. Preparation of Nitrogen-Doped Biochar and Its Adsorption Performance for Cr6+ and Pb2+ in Aqueous Systems. *Toxics*. 2025;13(5):402.

37. Ashebir H, Tibebu S, Bedada D, Fito J, Kassahun E, Worku A. Advanced methylene blue adsorption with a tailored biochar/graphene oxide/magnetite nanocomposite: characterization, optimization, and reusability. *Biomass Convers Biorefinery*. Published online 2024:1-22.

38. Birhanu A, Hailu AM, Worku Z, Tessema I, Angassa K, Tibebu S. Optimization of pyrolysis conditions for Catha edulis waste-based biochar production using response

surface methodology. *Bioresour Bioprocess*. 2025;12(1):1-18.

39. Kassahun E, Fito J, Tibebu S, et al. The Application of the Activated Carbon from Cordia africana Leaves for Adsorption of Chromium (III) from an Aqueous Solution. *J Chem*. 2022;2022.

40. Adhikari S, Mahmud MAP, Nguyen MD, Timms W. Evaluating fundamental biochar properties in relation to water holding capacity. *Chemosphere*. 2023;328:138620.

41. Mukherjee A, Lal R. Biochar impacts on soil physical properties and greenhouse gas emissions. *Agronomy*. 2013;3(2):313-339.

42. Ewunetu T, Selassie YG, Molla E, Admase H, Gezahegn A. Soil properties under different land uses and slope gradients: Implications for sustainable land management in the Tach Karnuary watershed, Northwestern Ethiopia. *Front Environ Sci*. 2025;13:1518068.

43. Mukhlisin M, Astuti HW, Wardihani ED, Matlan SJ. Techniques for ground-based soil moisture measurement: a detailed overview. *Arab J Geosci*. 2021;14:1-34.

44. Adhikari S, Timms W, Mahmud MAP. Optimising water holding capacity and hydrophobicity of biochar for soil amendment–A review. *Sci Total Environ*. 2022;851:158043.

45. Vieira CB, Silva GHMC, Almeida BG de, et al. Saturated Hydraulic Conductivity of Nine Soils According to Water Quality, Soil Texture, and Clay Mineralogy. *Agronomy*. 2025;15(4):864.

46. Omar MM, Shitindi MJ, Massawe BHJ, Pedersen O, Meliyo JL, Fue KG. Modeling the electrical conductivity relationship between saturated paste extract and 1: 2.5 dilution in different soil textural classes. *Front Soil Sci*. 2024;4:1421661.

47. Rihayat T, Salim S, Arlina A, et al. Determination of CEC value (Cation Exchange Capacity) of Bentonites from North Aceh and Bener Meriah. In: *Aceh Province.*

Indonesia Using Three Methods. IOP Conf. Series: Materials Science and Engineering. Vol 334. ; 2018.

48. Ratefinjanahary I, MacKenzie R, Sharma S, et al. Development of soil organic carbon quantification model and comparison based on CHN Analyser, Loss on Ignition, and Walkley-Black methods for mangrove soils in Madagascar. *Estuar Coast Shelf Sci*. Published online 2025:109182.

49. Bremner JM. Determination of nitrogen in soil by the Kjeldahl method. *J Agric Sci*. 1960;55(1):11-33.

50. Song S hui, Wen Y jie, Zhang J yao, Wang H. Rapid spectrophotometric measurement with a microplate reader for determining phosphorus in NaHCO3 soil extracts. *Microchem J*. 2019;146:210-213.

51. Chavan P, Kamble D, Pansare D, Shelke R, Rai M. Analysis of K and Na content of Soil samples by Flame Emission Photometry with other parameters. *Asian J Res Chem*. 2024;17(6):337-343.

52. Okalebo JR, Gathua KW, Woomer PL. Laboratory methods of soil and plant analysis: a working manual second edition. *Sacred Africa, Nairobi*. 2002;21:25-26.

53. Vanchikova E V, Shamrikova E V, Bespyatykh N V, et al. Comparative assessment of the methods for exchangeable acidity measuring. *Eurasian Soil Sci*. 2016;49(5):512-518.

54. Deshpande H. *Soil Physical Analysis: Tools and Techniques*. Educohack Press; 2025.

55. Da Silva Mendes J, Fernandes JD, Chaves LHG, Guerra HOC, Tito GA, de Brito Chaves I. Chemical and physical changes of soil amended with biochar. *Water, Air, Soil Pollut*. 2021;232(8):338.

56. Werdin J, Conn R, Fletcher TD, Rayner JP, Williams NSG, Farrell C. Biochar particle size and amendment rate are more important for water retention and weight of

green roof substrates than differences in feedstock type. *Ecol Eng*. 2021;171:106391.

57. Hussain R, Ravi K. Investigating biochar-amended soil as a potential lightweight material for embankments. *Ecol Eng*. 2022;180:106645.

58. Do PTM, Nguyen LX. A review of thermochemical decomposition techniques for biochar production. *Environ Dev Sustain*. Published online 2024:1-57.

59. Mishra RK, Mohanty K, Wang X. Pyrolysis kinetic behavior and Py-GC–MS analysis of waste dahlia flowers into renewable fuel and value-added chemicals. *Fuel*. 2020;260:116338.

60. He Y, Zhang S, Liu D, Xie X, Li B. Effect of biomass particle size on the torrefaction characteristics in a fixed-bed reactor. *Energies*. 2023;16(3):1104.

61. Altıkat A, Alma MH, Altıkat A, Bilgili ME, Altıkat S. A comprehensive study of biochar yield and quality concerning pyrolysis conditions: A multifaceted approach. *Sustainability*. 2024;16(2):937.

62. Torchia DF de O, Zonta E, de Andrade AM, Garcia AC. Production and characterization of biochar obtained from different biomass and pyrolysis temperature. *Brazilian J Chem Eng*. 2022;39(2):415-427.

63. Mariyam S, Alherbawi M, Pradhan S, Al-Ansari T, McKay G. Biochar yield prediction using response surface methodology: effect of fixed carbon and pyrolysis operating conditions. *Biomass Convers Biorefinery*. 2024;14(22):28879-28892.

64. Yang K, Wu K, Zhang H. Machine learning prediction of the yield and oxygen content of bio-oil via biomass characteristics and pyrolysis conditions. *Energy*. 2022;254:124320.

65. Wang T, Meng D, Zhu J, Chen X. Effects of pelletizing conditions on the structure of rice straw-pellet pyrolysis char. *Fuel*. 2020;264:116909.

66. Özbay G, Koçak E, Ahmad MS. Pyrolysis of water buffalo manure: Influence of temperature and alkali hydroxide additives on the quality of bio-oil. *Biocatal Agric Biotechnol*. 2021;38:102230.

67. Yang G, Wang Z, Xian Q, et al. Effects of pyrolysis temperature on the physicochemical properties of biochar derived from vermicompost and its potential use as an environmental amendment. *Rsc Adv*. 2015;5(50):40117-40125.

68. Handiso B, Pääkkönen T, Wilson BP. Effect of pyrolysis temperature on the physical and chemical characteristics of pine wood biochar. *Waste Manag Bull*. 2024;2(4):281-287.

69. Tripathi M, Sahu JN, Ganesan P. Effect of process parameters on production of biochar from biomass waste through pyrolysis: A review. *Renew Sustain energy Rev*. 2016;55:467-481.

70. Wu W, Mu L, Luo X, et al. Effect of temperature on synthesis of carbon quantum dots and biochar through one-step hydrothermal treatment of distillers' grains. *Ind Crops Prod*. 2025;227:120832.

71. Liu B, Wu Y, Xing Z, Zhang J, Xue Y. Optimization of Magnetic Biochar Preparation Process, Based on Methylene Blue Adsorption. *Molecules*. 2024;29(21):5213.

72. Iwuozor KO, Emenike EC, Bakare BF, et al. A review on the conversion of plant husk-based biomass into biochar. *Biofuels*. 2024;15(10):1331-1345.

73. Imran-Masood M, García-Díez E, Usman M, Lodhi BK, Waqas M, García S. Development of a novel bio char for CO2 capture and biogas upgrade: Static and dynamic testing. *J CO2 Util*. 2024;89:102958.

74. Babu KKBS, Nataraj M, Tayappa M, Vyas Y, Mishra RK, Acharya B. Production of biochar from waste biomass using slow pyrolysis: Studies of the effect of pyrolysis temperature and holding time on biochar yield and properties. *Mater Sci Energy*

Technol. 2024;7:318-334.

75. Alonge OI, Oloruntoba OA, Ogedengbe TS, Adedoja AM, Akintola IA. Optimization and Modeling of Process Parameters on Bio-Char Yield of Low-and High-density Sawdust for Solid Fuel. *J Renew Energy Environ*. 2024;11(3):42-51.

76. Sharma AK, Ghodke P, Sharma PK. Holistic utilization of Chlorella pyrenoidosa microalgae for extraction of renewable fuels and value-added biochar through in situ transesterification and pyrolysis reaction process. Biomass Convers Biorefinery 14: 5261–5274. Published online 2024.

77. Yu KL, Show PL, Ong HC, Ling TC, Chen WH, Salleh MAM. Biochar production from microalgae cultivation through pyrolysis as a sustainable carbon sequestration and biorefinery approach. *Clean Technol Environ Policy*. 2018;20(9):2047-2055.

78. Chintala V, Kumar S, Pandey JK, Sharma AK, Kumar S. Solar thermal pyrolysis of non-edible seeds to biofuels and their feasibility assessment. *Energy Convers Manag*. 2017;153:482-492.

79. Pradhan D, Singh RK, Bendu H, Mund R. Pyrolysis of Mahua seed (Madhuca indica)–Production of biofuel and its characterization. *Energy Convers Manag*. 2016;108:529-538.

80. Chaturvedi S, Singh SV, Dhyani VC, Govindaraju K, Vinu R, Mandal S. Characterization, bioenergy value, and thermal stability of biochars derived from diverse agriculture and forestry lignocellulosic wastes. *Biomass Convers Biorefinery*. 2023;13(2):879-892.

81. Jadhav A, Ahmed I, Baloch AG, et al. Utilization of oil palm fronds for bio-oil and bio-char production using hydrothermal liquefaction technology. *Biomass Convers Biorefinery*. 2021;11(5):1465-1473.

82. Yang X, Wang H, Strong PJ, et al. Thermal properties of biochars derived from waste

biomass generated by agricultural and forestry sectors. *Energies*. 2017;10(4):469.

83. Li X, Wang T, Chang SX, Jiang X, Song Y. Biochar increases soil microbial biomass but has variable effects on microbial diversity: A meta-analysis. *Sci Total Environ*. 2020;749:141593.

84. Costa CR, de Souza AM, dos Santos MGB, et al. Stability and carbon sequestration potential of bamboo biochar. *Biomass Convers Biorefinery*. Published online 2025:1-16.

85. Yeong KH, Liu T, Tan LT, Chew JJ, Wang Y. Study of the pyrolysis characteristics and soil amendment potential of palm mesocarp fiber, sago fiber coarse, and sago trunk bark in Malaysia. *J Soils Sediments*. Published online 2025:1-16.

86. Leng L, Huang H. An overview of the effect of pyrolysis process parameters on biochar stability. *Bioresour Technol*. 2018;270:627-642.

87. De Oliveira Paiva I, De Morais EG, Jindo K, Silva CA. Biochar N content, pools and aromaticity as affected by feedstock and pyrolysis temperature. *Waste and Biomass Valorization*. 2024;15(6):3599-3619.

88. Li L, Long A, Fossum B, Kaiser M. Effects of pyrolysis temperature and feedstock type on biochar characteristics pertinent to soil carbon and soil health: A meta-analysis. *Soil Use Manag*. 2023;39(1):43-52.

89. Chen J, Zhou J, Zheng W, et al. A complete review on the oxygen-containing functional groups of biochar: Formation mechanisms, detection methods, engineering, and applications. *Sci Total Environ*. Published online 2024:174081.

90. Yahaya SM, Mahmud AA, Abdullahi M, Haruna A. Recent advances in the chemistry of nitrogen, phosphorus and potassium as fertilizers in soil: A review. *Pedosphere*. 2023;33(3):385-406.

91. Solymos K, Babcsányi I, Ariya B, et al. Photocatalytic and surface properties of

titanium dioxide nanoparticles in soil solutions. *Environ Sci Nano*. 2024;11(3):1204-1216.

92. Zhao K, Yang Y, Zhang L, et al. Silicon-based additive on heavy metal remediation in soils: Toxicological effects, remediation techniques, and perspectives. *Environ Res*. 2022;205:112244.

93. Wang P, Zhang X, Zhang X, et al. Manganese oxide catalytic materials for degradation of organic pollutants in advanced oxidation processes: A review. *J Water Process Eng*. 2024;66:106048.

94. Zhang C, Zhao X, Liang A, et al. Insight into the soil aggregate-mediated restoration mechanism of degraded black soil via biochar addition: Emphasizing the driving role of core microbial communities and nutrient cycling. *Environ Res*. 2023;228:115895.

95. Ajagalla M, Pandey M, Choudhary J. Optimizing Fertilizer Recommendations for Root Vegetable Crops Through Soil Feature Analysis and Environmental Parameter Integration Via Machine Learning Techniques. In: *International Conference on Data Science and Applications*. Springer; 2025:377-387.

96. Kordrostami M, Ghasemi-Soloklui AA. Innovative applications of biochar in nuclear remediation and catalysis. *Biochar*. 2025;7(1):74.

97. Leng L, Xiong Q, Yang L, et al. An overview on engineering the surface area and porosity of biochar. *Sci Total Environ*. 2021;763:144204.

98. Muzyka R, Misztal E, Hrabak J, Banks SW, Sajdak M. Various biomass pyrolysis conditions influence the porosity and pore size distribution of biochar. *Energy*. 2023;263:126128.

99. Pasieczna-Patkowska S, Cichy M, Flieger J. Application of Fourier transform infrared (FTIR) spectroscopy in characterization of green synthesized nanoparticles. *Molecules*. 2025;30(3):684.

100. Sánchez-González A, Fuentes-García R, Pablo-Trujillo C, Hernández-Quiroz M, Ponce de León Hill CA. Sediment organic matter description from an urban wetland: multivariate analysis of FT-IR bands to determine its origin. *Int J Environ Anal Chem*. 2021;101(7):1007-1025.

101. Esposito VJ, Allamandola LJ, Boersma C, et al. Anharmonic IR absorption spectra of the prototypical interstellar PAHs phenanthrene, pyrene, and pentacene in their neutral and cation states. *Mol Phys*. 2024;122(7-8):e2252936.

102. Senathirajah K, Kandaiah R, Panneerselvan L, Young K, Palanisami T. Disinfection impacts: Effects of different disinfection treatments on common polymer types to guide the identification of polymers of concern in the water industry. *Cambridge Prism Plast*. 2025;3:e9.

103. Subbiah N, Palanisamy T. Harnessing Protein Waste into Reduced Graphitic Carbon Oxide-Copper-Collagen Nanocomposite for Visible Light Photocatalytic Degradation of Nano Plastics. *Adv Sustain Syst*. 2024;8(7):2300487.

104. Ani PC, Al-Abedi HJ, Smith JD, Zeitoun Z. Biochar Surface Chemistry Modification by Blending Hardwood, Softwood, and Refuse-Derived Fuel: Insights from XPS, FTIR, and Zeta Potential Analysis. *Fuels*. 2025;6(3):71.

105. Devi M, Pandey P, Sharma S. Crystalline–disordered–crystalline transition in nitrogen–carbon materials. *J Appl Phys*. 2025;137(2).

106. Xue H, Dong X, Fan Y, Ma X, Yao S. Study of structural transformation and chemical reactivity of kaolinite-based high ash slime during calcination. *Minerals*. 2023;13(4):466.

107. Yakout SM. Physicochemical characteristics of biochar produced from rice straw at different pyrolysis temperature for soil amendment and removal of organics. *Proc Natl Acad Sci India Sect A Phys Sci*. 2017;87(2):207-214.

108. Ajay PD, Ganesha A, Girish H, Kumar N, Kumar S, Suranjan Salins S. Development of surface-modified rice husk adsorbents for eco-friendly industrial desiccation. *Int J Sustain Energy*. 2025;44(1):2543819.

109. Yilmaz B, Kamperidou V, Akcay SB, Kar T, Fazli H, Varol T. Characterization of Low-Temperature Waste-Wood-Derived Biochar upon Chemical Activation. *Forests*. 2025;16(8):1237.

110. Apaydın Varol E, Mutlu Ü. TGA-FTIR analysis of biomass samples based on the thermal decomposition behavior of hemicellulose, cellulose, and lignin. *Energies*. 2023;16(9):3674.

111. Xu Z, He M, Xu X, Cao X, Tsang DCW. Impacts of different activation processes on the carbon stability of biochar for oxidation resistance. *Bioresour Technol*. 2021;338:125555.

112. Johnson Jeyaraj N, Sankararajan V. Water hyacinth biomass-based biochar: Preparation and characterizations for sustainable soil amendment. *Int Rev Appl Sci Eng*. 2025;16(2):182-192.

113. Chen D, Fang Z, Wei Y, et al. Micro-Raman spectroscopy and Petrography for unraveling the complex heterogeneous physicochemical structures of biochar from the scale of bulk to micro: A comparison and discussion. *J Anal Appl Pyrolysis*. 2025;188:107057.

114. da Rocha AR, Soares FLF, Mangrich AS, Pantano G. Synergetic effect of heating rate, temperature, and residence time of modified agro-industrial waste biochars on phosphate adsorption. *Int J Environ Sci Technol*. 2025;22(6):4203-4214.

115. Claoston N, Samsuri AW, Ahmad Husni MH, Mohd Amran MS. Effects of pyrolysis temperature on the physicochemical properties of empty fruit bunch and rice husk biochars. *Waste Manag Res*. 2014;32(4):331-339.

116. Li Z, Zhang L, Amirkhiz BS, et al. Carbonized chicken eggshell membranes with 3D architectures as high-performance electrode materials for supercapacitors. *Adv Energy Mater*. 2012;2(4):431-437.

117. Kołtowski M, Hilber I, Bucheli TD, Charmas B, Skubiszewska-Zięba J, Oleszczuk P. Activated biochars reduce the exposure of polycyclic aromatic hydrocarbons in industrially contaminated soils. *Chem Eng J*. 2017;310:33-40.

118. Kim Y, Oh JI, Vithanage M, Park YK, Lee J, Kwon EE. Modification of biochar properties using CO2. *Chem Eng J*. 2019;372:383-389.

119. Yin Y, Gao Y, Li A. Self-activation of biochar from furfural residues by recycled pyrolysis gas. *Waste Manag*. 2018;77:312-321.

120. Jiang TJ, Morgan Jr HM, Tsai WT, Chien H, Yen TB, Lee YR. Thermochemical conversion of biomass into biochar: enhancing adsorption kinetics and pore properties for environmental sustainability. *Sustainability*. 2024;16(15):6623.

121. Cárdenas-Aguiar E, Méndez A, Gascó G, Lado M, Paz-González A. The effects of feedstock, pyrolysis temperature, and residence time on the properties and uses of biochar from broom and gorse wastes. *Appl Sci*. 2024;14(10):4283.

122. Guo M, Song W, Tian J. Biochar-facilitated soil remediation: mechanisms and efficacy variations. *Front Environ Sci*. 2020;8:521512.

123. Liu S, Cen B, Yu Z, Qiu R, Gao T, Long X. The key role of biochar in amending acidic soil: reducing soil acidity and improving soil acid buffering capacity. *Biochar*. 2025;7(1):52.

124. Wang Y, Wang HS, Tang CS, Gu K, Shi B. Remediation of heavy-metal-contaminated soils by biochar: a review. *Environ Geotech*. 2019;9(3):135-148.

125. Singh S, Swami S, Gogoi J, et al. Effect of biochar-mediated treatments on the improvement of soil acidity, crop performance and soil properties. *Ama, Agric Mech*

Asia, Africa Lat Am. 2023;54:13575-13603.

126. Premalatha RP, Poorna Bindu J, Nivetha E, et al. A review on biochar's effect on soil properties and crop growth. *Front Energy Res*. 2023;11:1092637.

127. Abbas T, Rizwan M, Ali S, et al. Effect of biochar on alleviation of cadmium toxicity in wheat (Triticum aestivum L.) grown on Cd-contaminated saline soil. *Environ Sci Pollut Res*. 2018;25:25668-25680.

128. Sun X, Shan R, Li X, et al. Characterization of 60 types of Chinese biomass waste and resultant biochars in terms of their candidacy for soil application. *Gcb Bioenergy*. 2017;9(9):1423-1435.

129. Askeland M, Clarke B, Paz-Ferreiro J. Comparative characterization of biochars produced at three selected pyrolysis temperatures from common woody and herbaceous waste streams. *PeerJ*. 2019;7:e6784.

130. Santos M, Morim AC, Videira M, Silva F, Matos M, Tarelho LAC. Characteristics of Biochar Obtained by Pyrolysis of Residual Forest Biomass at Different Process Scales. *Energies (19961073)*. 2024;17(19).

131. Zhang H, Cheng Y, Zhong Y, Ni J, Wei R, Chen W. Roles of biochars' properties in their water-holding capacity and bound water evaporation: quantitative importance and controlling mechanism. *Biochar*. 2024;6(1):30.

132. Suliman W, Harsh JB, Abu-Lail NI, Fortuna AM, Dallmeyer I, Garcia-Perez M. Influence of feedstock source and pyrolysis temperature on biochar bulk and surface properties. *Biomass and Bioenergy*. 2016;84:37-48.

133. Ahmad M, Rajapaksha AU, Lim JE, et al. Biochar as a sorbent for contaminant management in soil and water: a review. *Chemosphere*. 2014;99:19-33.

134. Munera-Echeverri JL, Martinsen V, Strand LT, Zivanovic V, Cornelissen G, Mulder J. Cation exchange capacity of biochar: An urgent method modification. *Sci Total*

Environ. 2018;642:190-197.

135. Yuan JH, Xu RK, Zhang H. The forms of alkalis in the biochar produced from crop residues at different temperatures. *Bioresour Technol*. 2011;102(3):3488-3497.

136. Antonangelo JA, Culman S, Zhang H. Comparative analysis and prediction of cation exchange capacity via summation: influence of biochar type and nutrient ratios. *Front Soil Sci*. 2024;4:1371777.

137. Sharma P. Biochar application for sustainable soil erosion control: a review of current research and future perspectives. *Front Environ Sci*. 2024;12:1373287.

138. Villa-Parejo J, Aguirre-Forero S, Piraneque-Gambasica N, Cruz-O'Byrne R. Enhancing soil properties and plant growth with coffee and oil palm biochar: A sustainable circular economy approach in agroindustry. *Ind Crops Prod*. 2025;233:121491.

139. Eduah JO, Nartey EK, Abekoe MK, Asomaning SK, Essibu JK, Henriksen SW. Acidity and aluminum speciation in biochar amended tropical soils. *Commun Soil Sci Plant Anal*. 2022;53(7):913-927.

140. Ahmad MN, Anuar MI, Abd Aziz N, Murdi AA. Function and application of Soil Electrical Conductivity (EC) sensor in agriculture: A Review. *Adv Agric Food Res J*. 2025;6(1).

141. Dey S, Purakayastha TJ, Sarkar B, et al. Enhancing cation and anion exchange capacity of rice straw biochar by chemical modification for increased plant nutrient retention. *Sci Total Environ*. 2023;886:163681.

142. Gross A, Bromm T, Glaser B. Soil organic carbon sequestration after biochar application: A global meta-analysis. *Agronomy*. 2021;11(12):2474.

143. Jia Y, Hu Z, Ba Y, Qi W. Application of biochar-coated urea controlled loss of fertilizer nitrogen and increased nitrogen use efficiency. *Chem Biol Technol Agric*. 2021;8(1):3.

144. Elbana TA, Bakr N, Shahin SA, Azab NAA, El-Ashry SM. Influence of acidified-biochar on phosphorus and potassium availability in alkaline sandy soil. *Sci Rep*. 2025;15(1):30504.

145. He D, Liu X, Hu D, et al. Density functional theory calculation for understanding the roles of biochar in immobilizing exchangeable Al3+ and enhancing soil quality in acidic soils. *Ecotoxicol Environ Saf*. 2025;290:117630.

146. Yuan Q, Gao Y, Ma G, et al. The long-term effect of biochar amendment on soil biochemistry and phosphorus availability of calcareous soils. *Agriculture*. 2025;15(5):458.

147. Zhu Z, Zhang Y, Tao W, Zhang X, Xu Z, Xu C. The Biological Effects of Biochar on Soil's Physical and Chemical Characteristics: A Review. *Sustainability*. 2025;17(5):2214.

148. Verheijen FGA, Zhuravel A, Silva FC, Amaro A, Ben-Hur M, Keizer JJ. The influence of biochar particle size and concentration on bulk density and maximum water holding capacity of sandy vs sandy loam soil in a column experiment. *Geoderma*. 2019;347:194-202.

149. Blanco-Canqui H. Biochar and soil physical properties. *Soil Sci Soc Am J*. 2017;81(4):687-711.

150. Liu Z, Dugan B, Masiello CA, Barnes RT, Gallagher ME, Gonnermann H. Impacts of biochar concentration and particle size on hydraulic conductivity and DOC leaching of biochar–sand mixtures. *J Hydrol*. 2016;533:461-472.

151. Hussain R, Kumar H, Bordoloi S, et al. Effect of biochar type and amendment rates on soil physicochemical properties: potential application in bioengineered structures. *Adv Civ Eng Mater*. 2024;13(1):1-20.

152. Ghorbani M, Amirahmadi E, Zamanian K. In-situ biochar production associated with

paddies: Direct involvement of farmers in greenhouse gases reduction policies besides increasing nutrients availability and rice production. *L Degrad Dev*. 2021;32(14):3893-3904.

153. Singh H, Northup BK, Rice CW, Prasad PVV. Biochar applications influence soil physical and chemical properties, microbial diversity, and crop productivity: a meta-analysis. *Biochar*. 2022;4(1):8.

154. Dume B, Ayele D, Regassa A, Barecha G. Interactive effects of biochar in soil related to feedstock and pyrolysis temperature. *Am J Agric Environ Sci*. 2016;16(3):442-448.

155. Zhang Y, Idowu OJ, Brewer CE. Using agricultural residue biochar to improve soil quality of desert soils. *Agriculture*. 2016;6(1):10.

156. Garbuz S, Mackay A, Camps-Arbestain M, DeVantier B, Minor M. Biochar amendment improves soil physico-chemical properties and alters root biomass and the soil food web in grazed pastures. *Agric Ecosyst Environ*. 2021;319:107517.

157. Naveed M, Schjønning P, Keller T, de Jonge LW, Moldrup P, Lamandé M. Quantifying vertical stress transmission and compaction-induced soil structure using sensor mat and X-ray computed tomography. *Soil Tillage Res*. 2016;158:110-122.

158. Six J, Bossuyt H, Degryze S, Denef K. A history of research on the link between (micro) aggregates, soil biota, and soil organic matter dynamics. *Soil tillage Res*. 2004;79(1):7-31.